HHS Public Access

Author manuscript

Cell. Author manuscript; available in PMC 2019 August 23.

Published in final edited form as:

Cell. 2018 August 23; 174(5): 1200–1215.e20. doi:10.1016/j.cell.2018.07.015.

Nuclear Pores Promote Lethal Prostate Cancer by Increasing POM121-Driven E2F1, MYC, and AR Nuclear Import

Veronica Rodriguez-Bravo[1,2,3,*], **Raffaella Pippa**[1,2,3], **Won-Min Song**[4,5], **Marc Carceles-Cordon**[3], **Ana Dominguez-Andres**[1,2,3], **Naoto Fujiwara**[5], **Jungreem Woo**[1,2,3], **Anna P. Koh**[5], **Adam Ertel**[1], **Ravi K. Lokareddy**[6], **Alvaro Cuesta-Dominguez**[7,8], **Rosa S. Kim**[5], **Irene Rodriguez-Fernandez**[3], **Peiyao Li**[1,2], **Ronald Gordon**[3], **Hadassa Hirschfield**[5], **Josep M. Prats**[9], **E. Premkumar Reddy**[7], **Alessandro Fatatis**[10], **Daniel P. Petrylak**[11], **Leonard Gomella**[12], **W. Kevin Kelly**[1,2,12], **Scott W. Lowe**[13], **Karen E. Knudsen**[1,2,12], **Matthew D. Galsky**[14], **Gino Cingolani**[6], **Amaia Lujambio**[7,8], **Yujin Hoshida**[5], and **Josep Domingo-Domenech**[1,2,3,15,*]

[1]Cancer Biology Department, Sidney Kimmel Cancer Center, Thomas Jefferson University, Philadelphia, PA 19107, USA

[2]Medical Oncology Department, Sidney Kimmel Cancer Center, Thomas Jefferson University, Philadelphia, PA 19107, USA

[3]Pathology Department, Icahn School of Medicine at Mount Sinai, New York, NY 10029, USA

[4]Genetic and Genomic Sciences Department. Icahn School of Medicine at Mount Sinai, New York, NY 10029, USA

[5]Liver Tumor Translational Research Program, Simmons Comprehensive Cancer Center, University of Texas Southwestern Medical Center, Dallas, TX 75390, USA

[6]Department of Biochemistry and Molecular Biology, Sidney Kimmel Cancer Center, Thomas Jefferson University, Philadelphia, PA 19107, USA

[7]Oncological Sciences Department. Icahn School of Medicine at Mount Sinai, New York, NY 10029, USA

[8]Division of Liver Diseases, Medicine Department, Icahn School of Medicine at Mount Sinai, New York, NY 10029, USA

[*]Correspondence: veronica.rodriguez-bravo@jefferson.edu (V.R.-B.), josep.domingo-domenech@jefferson.edu (J.D.-D.).

AUTHOR CONTRIBUTIONS

R.P., M.C.-C., A.D.-A., J.W., I.R.-F., and P.L. performed and analyzed *in vitro* and *in vivo* experiments. W.-M.S., A.P.K., R.S.K., H.H., N.F., A.E., and Y.H. analyzed computational studies. Y.H., E.P.R., D.P.P., A.F., L.G., K.E.K., and M.D.G. helped in design the study. A.C.-D., S.W.L., and A.L. generated shRNA probes. R.G. performed and analyzed high resolution TEM experiments. R.K.L. and G.C. provided proteins for *in vitro* protein binding assays. J.M.P., W.K.K., and M.D.G. provided human specimens. V.R.-B. and J.D.-D. conceived the project, supervised experiments, analyzed data, and wrote the paper.</author_notes>

DECLARATION OF INTERESTS

The authors declare no competing interests.

DATA AND SOFTWARE AVAILABILITY

The accession number for the datasets reported in this paper is GEO: GSE103637. Other accession numbers used in this study are GEO: GSE58966 and GSE35988, dbGaP: phs000447.v1.p1, and dbGap: phs000915.v1.p1.

SUPPLEMENTAL INFORMATION

Supplemental Information includes seven figures and five tables and can be found with this article online at https://doi.org/10.1016/j.cell.2018.07.015.

[9]Urology Department, Hospital de Calella, Barcelona 08370, Spain

[10]Pharmacology and Physiology Department, Drexler University, Philadelphia, PA 19104, USA

[11]Medical Oncology Department, Yale Comprehensive Cancer Center, Yale School of Medicine, New Haven, CT 06520, USA

[12]Urology Department, Sidney Kimmel Cancer Center, Thomas Jefferson University, Philadelphia, PA 19107, USA

[13]Cancer Biology and Genetics Program, Memorial Sloan Kettering Cancer Center, New York, NY 10065, USA

[14]Medical Oncology Department, Icahn School of Medicine at Mount Sinai, New York, NY 10029, USA

[15]Lead Contact

SUMMARY

Nuclear pore complexes (NPCs) regulate nuclearcytoplasmic transport, transcription, and genome integrity in eukaryotic cells. However, their functional roles in cancer remain poorly understood. We interrogated the evolutionary transcriptomic landscape of NPC components, nucleoporins (Nups), from primary to advanced metastatic human prostate cancer (PC). Focused loss-of-function genetic screen of topupregulated Nups in aggressive PC models identified POM121 as a key contributor to PC aggressiveness. Mechanistically, POM121 promoted PC progression by enhancing importin-dependent nuclear transport of key oncogenic (E2F1, MYC) and PC-specific (ARGATA2) transcription factors, uncovering a pharmacologically targetable axis that, when inhibited, decreased tumor growth, restored standard therapy efficacy, and improved survival in patient-derived pre-clinical models. Our studies molecularly establish a role of NPCs in PC progression and give a rationale for NPC-regulated nuclear import targeting as a therapeutic strategy for lethal PC. These findings may have implications for understanding how NPC deregulation contributes to the pathogenesis of other tumor types.

In Brief

POM121- and importin β-mediated nuclear import of a subset of oncogenic transcription factors promotes prostate cancer aggressiveness and reveals a pharmacologically targetable dependency.

Graphical Abstract

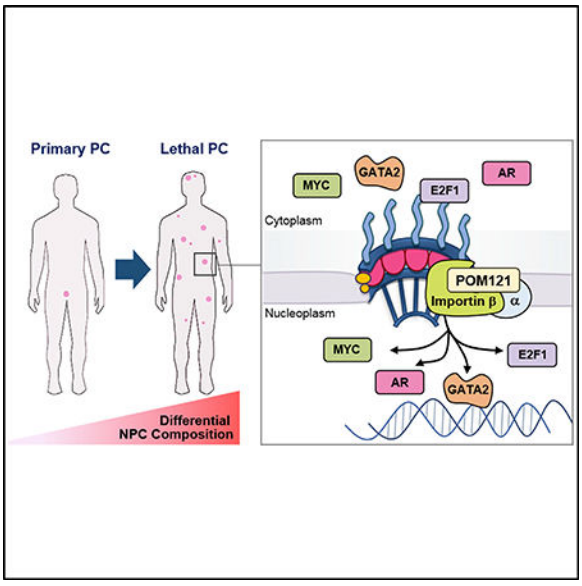

INTRODUCTION

Nuclear pore complexes (NPCs) are large transmembrane cylinders that perforate the nuclear envelope (NE) formed of around 30 types of proteins called nucleoporins (Nups) (Knockenhauer and Schwartz, 2016). Expression of Nups varies throughout ontogeny and among different cell types and tissues (Raices and D'Angelo, 2012). As defining features of the eukaryotic cell, NPCs are known to regulate and participate in a plethora of functions that are essential for the cell, such as cell-cycle/mitotic regulation (Rodriguez-Bravo et al., 2014), transcriptional activation (Taddei et al., 2006), RNA processing (Rougemaille et al., 2008), gene silencing (Van de Vosse et al., 2013), and heterochromatin modulation (Blobel, 1985; Brickner and Brickner, 2012; Light et al., 2010; Pascual-Garcia and Capelson, 2014). Among these, the NPCs have been shown to have a pivotal regulatory function in protein and RNA transport across the NE (Wente and Rout, 2010). On a collective effort to understand its molecular underpinnings, many key molecules have been found to regulate nucleocytoplasmatic transport. These include GTPase Ran, which regulates nucleocytoplasmic transport in interphase, and karyopherins, a superfamily of transport receptors that bind to their cargoes by recognition of specific nuclear localization or nuclear export signals and facilitate canonical transport by forming transient interactions with the NPC (Pemberton and Paschal, 2005).

Of interest, several Nups have been linked to tumor formation and progression (Chow et al., 2012; Ko¨ hler and Hurt, 2010; Simon and Rout, 2014), suggesting that NPC composition and function may be of relevance for cancer pathogenesis. In this context, Nups have been identified in a wide range of chromosomal translocations that constitutively activate kinases, while other studies evidence the downregulation or overexpression of Nups in a range of tumor types. In truth, however, the specific Nups and Nup-based mechanisms contributing to cancer aggressiveness remain to be investigated.

A classic example of the intractability and consequent lethality of aggressive tumors is found in prostate cancer (PC). PC is the most frequent tumor and a leading cause of cancer death in men worldwide (Torre et al., 2015), and even though most patients are diagnosed at early stages and can be cured with local therapy, a subset (~10%–15%) relapse and progress to an advanced metastatic lethal state (Pound et al., 1999). In this context, several treatment options that include androgen withdrawal (Seidenfeld et al., 2000), anti-androgen therapy (Beer et al., 2014; de Bono et al., 2011; Ryan et al., 2013; Scher et al., 2012), and taxane chemotherapy (de Bono et al., 2010; Petrylak et al., 2004; Sweeney et al., 2015; Tannock et al., 2004) may improve patient's survival. However, many of these patients develop uniformly fatal therapy-resistant PC. These devastating clinical outcomes are further evidence of the current deficiency of knowledge on the mechanisms that control PC progression to advanced aggressive lethal stages and highlight the urgent need to dissect the molecular mechanisms that drive its aggressiveness and identify targets to improve PC patient's clinical outcome.

Based on this, together with the underlying evidence that links the NPC with cancer pathogenesis, we aimed to study if specific Nups and NPC-Nup based mechanisms contribute to PC aggressiveness. In this study, we have found that NPC composition is substantially modified in tumors that progress to an advanced disease, and specific Nups enhance the signaling activity of oncogenic and PC-specific transcription factors. In particular, the increased expression of Nup POM121 selectively promotes importin-mediated nuclear transport of MYC, E2F1, AR, and GATA2 that propel the tumor initiating, proliferation, and survival properties of PC cells. Notably, genetic and pharmacologic inhibition of the POM121-importin β axis significantly diminishes these biological properties. Collectively, these results mechanistically define the role of the NPC in the progression of PC into an aggressive lethal state and identify a potential therapeutic strategy for this devastating disease.

RESULTS

NPCs Display a Distinct Nup Composition that Promotes Tumor Aggressiveness in Lethal PC

To investigate the Nups involved in the aggressiveness of PC, we initially scrutinized the evolutionary landscape of NPC composition by interrogating gene expression profiles of Nups in a dataset containing primary and warm autopsy PC tumor samples (Grasso et al., 2012) and identified a subset of Nups that are distinctively deregulated in lethal disease (Figure 1A). Next, we investigated if the observed changes in Nup expression were associated to modifications in nuclear envelope (NE) structure and NPC number during PC progression to an aggressive stage. High resolution transmission electron microscopy (TEM) imaging analysis of primary and metastatic prostate tumor cells (Table S1) confirmed classical morphological features associated to aggressiveness in cancer cells (Dey, 2010; Rashid and Ul Haque, 2011), such as prominent NE invaginations (Figure 1B), increased number of NPCs (Figure 1C), and increased NE spacing (Figure 1D) when compared to primary tumor PC cells.

To evaluate the functional role of overexpressed Nups in lethal PC, we performed a focused loss-of-function genetic screen (Figure S1A) of the 7 Nups most significantly increased in warm autopsy tumor samples (Figure 1A) in two chemotherapy (docetaxel) and castration resistant PC cell lines, DU145-DR and 22Rv1-DR, which mimic the high tumorigenicity and multidrug resistant phenotype of advanced lethal PC (DomingoDomenech et al., 2012) and their parental, DU145 and 22Rv1, counterparts. Reproducing what is observed in advanced PC patient's tumor samples, these cellular models (DU145-DR and 22Rv1-DR) also exhibited an increase in the mRNA levels in 6 of the 7 clinically upregulated Nups when compared to parental cells (Figure S1B). After assessing successful knockdown of each Nup (mRNA decrease >80%) using two independent small interfering RNAs (siRNAs) (Figure S1C), we identified 4 Nups (POM121, NUP210, NUP62, and TPR) impacting on soft agar colony formation (Figure 1E), 4 Nups (POM121, NUP214, NUP62, and TPR) affecting proliferation (Figure 1F), and two Nups (POM121 and TPR) impinging on response to standard therapy (Figures 1G and S1D) of aggressive PC cells. Notably, functional genetic studies on parental cells, DU145 and 22Rv1, only showed a consistent impact of NUP62 on tumorigenesis and proliferation (Figures S1E–S1G). Thus, these results suggest that during PC progression to an advanced aggressive lethal stage, cancer cells significantly modify their NPC composition, with a subset of specific Nups selectively contributing to the aggressiveness of PC cells.

POM121 Regulates Tumorigenesis, Proliferation, and Survival in Lethal PC

We next focused on dissecting the role of POM121 in advanced stage PC, because this Nup is the most upregulated in human advanced lethal prostate tumor samples and its knockdown exhibited the strongest effects specifically in aggressive PC cells. POM121 is a 121 kDa transmembrane Nup that participates in NPC assembly through its N-terminal domain (Antonin et al., 2005; Doucet et al., 2010; Talamas and Hetzer, 2011). Immunohistochemistry (Figures 2A and S2A) and high resolution TEM imaging (Figure 2B) analyses of POM121 in primary and advanced PC tissue samples revealed that its expression was higher in the NPCs of advanced tumor cells and at the protein level in aggressive PC cells when compared to parental cells (Figure 2C). Next, we investigated if the phenotype observed after POM121 depletion was due to a major structural disruption of the NPC. Transient POM121 knockdown did not affect the protein expression levels (Figure S2B) and NPC localization (Figure 2D) of other Nups (i.e., NUP214, NUP98, and NUP62). TEM imaging analysis confirmed this result in our experimental models, no major changes were found in NE spacing and number of nuclear pores (Figure S2C). Of note, NPC integrity remained unaltered after prolonged POM121 depletion (Figures S2D–S2F), suggesting that in PC cells the NPC can assemble or persist under POM121-depleted conditions, as described previously in other cellular models (Stavru et al., 2006). We also further explored the on-target effects of POM121 siRNA by stably expressing a siRNA-resistant POM121 (Figure S2G) that rescued the previously observed effects on soft agar colony formation (Figure S2H), proliferation (Figure S2I), and response to standard therapy (Figure S2J). These results verified that the POM121 knockdown phenotype was specific and did not occur because of a disassembly of the NPC. Concurrently, gain-offunction studies by overexpression of POM121 in parental cells (Figure 2E) increased the soft agar colony formation (Figure 2F), proliferation (Figure 2G), and number of colonies after standard

therapy exposure (Figure 2H), when compared to controls in which parental cells where transduced with an empty or NUP62 vectors (Figures 2E–2H), further suggesting that POM121 upregulation selectively increases the aggressiveness of PC cells. In addition, *in vivo* studies were performed by injecting mice with highly tumorigenic DU145-DR and 22Rv1-DR PC cells stably expressing inducible short hairpin RNAs (shRNAs) against POM121 (Figure 3A) and, upon doxycycline induction (Figures 3B and S3A), tumor incidence reduced (Figures 3C and S3B), tumor growth decreased, and efficacy of standardof-care chemotherapy increased in established xenografts (Figure 3D). Notably, tumors with lower levels of POM121 displayed a decrease in the proliferation marker Ki67 (Figure 3E) and increased cleaved caspase 3 expression when treated with standard chemotherapy (Figures 3F and S3C). Collectively, these results suggest that POM121 has a key role in promoting PC aggressiveness and provided the overarching rational to further dissect the mechanisms through which POM121 exerts these effects.

Nuclear Import Is Modulated by POM121 in Aggressive PC Cells

Having asserted that POM121 has a critical role in regulating PC aggressiveness properties, we decided to further analyze the molecular mechanisms associated to POM121 function. It seemed plausible that POM121 expression in PC cells had effects in nuclear transport, because POM121 contains a repetitive pentapeptide motif XFXFG in the C terminus domain (Hallberg et al., 1993) and POM121 interacts with import transport receptors in *Xenopus* extracts (Yavuz et al., 2010). Indeed, POM121 knockdown in PC cells stably expressing a glucocorticoid receptor-GFP (GR-GFP) reporter resulted in a decrease of nuclear import of GR-GFP after dexamethasone treatment (Figure 4A). Immunoblot analysis on separate nuclear and cytoplasmic fractions confirmed this result (Figure S4A).

When assessing the interaction between POM121 and the import machinery, immunoprecipitation assays showed that, at equal levels of importin β, aggressive cells displayed an increased binding of POM121 protein when compared with their parental, less aggressive, counterparts (Figure 4B), a result that was also observed in reverse immunoprecipitation of POM121 protein with importin β (Figure S4B). Consistently, we observed that aggressive PC cells displayed a more efficient nuclear import of GR-GFP when compared to parental cells (Figure S4C). Crucially, opposing what is observed when expressing a siRNAresistant $POM121^{wt}$ in PC cells, under POM121 knockdown conditions, expression of a siRNA-resistant POM121 mutant (Figure S4D), $POM121^{\Delta NPC}$, that does not localize to the NPC (Figure 4C) and does not interact with importin β (Figure 4D), failed to rescue the effects on tumorigenesis (Figure 4E), proliferation (Figure 4F), and response to standard therapy (Figure 4G). Therefore, suggesting that both POM121 NPC localization and importin β interaction are necessary for its functional effects.

Next, we investigated if the interaction between POM121 and importin β was direct or mediated by other FG-Nups (NUP62, NUP153, and NUP98). Interestingly, we observed that the increase of POM121 in aggressive cells was not related to an increase in these FG-Nups (Figure S4E). These results are in line with transcriptomic data from PC patients (Figure 1A), wherein a *POM121* increase in warm autopsy patients is not paralleled by an increase in other FG-Nups. Moreover, overexpression of POM121 in parental PC cells did not alter

the expression of other FG-Nups (Figure S4F), and neither did POM121 knockdown in aggressive PC cells (Figure S4G). Immunoprecipitation assays showed that POM121 increases its binding to importin b in aggressive cells, whereas other FG-Nups do not (Figure 4H). Notably, $POM121^{wt}$, and not $POM121^{\Delta NPC}$, directly binds to importins through its NLS in *in vitro* assays (Figures 4I, S4H, and S4I).

Moreover, conscious that POM121 plays a key role in NPC assembly (Antonin et al., 2005; Doucet et al., 2010; Talamas and Hetzer, 2011), we investigated if the overexpression of POM121 would increase the number of NPCs. Indeed, TEM imaging analysis revealed that the number of NPCs was augmented in PC cells stably overexpressing POM121 when compared to controls (Figure 4J). Notably, this result was in concordance with the increase in number of pores observed in tumor cells from metastatic tumor samples compared to primary tumor samples (Figure 1C). Thus, jointly these results suggest that upregulated POM121 levels at the nuclear pore enhance nuclear import by selectively increasing the binding to the import machinery and by raising the number of NPCs in aggressive PC cells.

POM121 Enhances Oncogenic and PC-Related Signaling Pathways

To further dissect the molecular events following POM121 function, we performed transcriptome profiling by RNA-sequencing of POM121-depleted DU145-DR and 22Rv1-DR cells and defined a common functional POM121 target gene signature (Figure 5A; Table S2). Gene ontology analysis revealed that POM121 gene signature was associated to biological processes such as cellular death, proliferation, and differentiation (Figure S5A). An unbiased survey of transcriptome meta-analysisbased functional target gene signature database (Liberzon et al., 2015) elucidated distinct induction of the target gene signatures of oncogenic transcription factors MYC and E2F1 in the control cells with intact POM121 compared to POM121 knockdown cells (Figure 5B; Tables S3 and S4).

MYC and E2F1 are transcription factors transported into the nucleus (Dang and Lee, 1988; Ivanova et al., 2007; Wang et al., 2012) that contribute to PC aggressiveness (Ellwood-Yen et al., 2003; Hawksworth et al., 2010; Liang et al., 2016; Thompson et al., 1989; Zheng et al., 2009). Consistent with this result, functional target gene signatures of POM121, MYC, and E2F1, as well as other experimentally defined target gene signatures of MYC and E2F1 defined in the literature (Table S5) were significantly induced in warm autopsy PC tissues (Figure 5C). Pointing to a potential role of POM121 in regulating nuclear transport of these transcription factors, we initially found that importin b binds to E2F1 and MYC in PC cells (Figure S5B). Indeed, immunoblot analysis on separate nuclear and cytoplasmic fractions of control and POM121 knockdown on DU145-DR and 22Rv1-DR cells further portrayed that nuclear import of MYC and E2F1 were decreased when POM121 was depleted (Figure 5D). Notably, we confirmed that the localization effects on these transcription factors where specific and not due to a loss of NE integrity after POM121 depletion, because the nuclear and cytoplasmic localization of two proteins, hnRNP-A1 and b-catenin, which nuclear transport is not dependent on importin b (Jamieson et al., 2014; Pollard et al., 1996) remained unaltered (Figure 5E). Moreover, supporting the specificity of POM121 in regulating nuclear transport of these transcription factors, we observed that parental cells overexpressing POM121 increased the nuclear localization of MYC and E2F1, whereas the

nuclear localization of b-catenin was not affected (Figure 5F). Taken together, these results suggest that POM121 modulates the importin b-dependent nuclear localization and signaling activity of specific transcription factors.

Mindful of the critical role of the androgen receptor (AR) as a crucial driver of PC progression (Knudsen and Penning, 2010), and considering that its nuclear import is mediated by importin b (Cutress et al., 2008; Georget et al., 1997), we next extended our studies to explore if POM121 regulates AR nuclear localization and signaling activity in the AR-expressing 22Rv1-DR cells. Indeed, POM121 knockdown decreased AR localization in the nucleus (Figure 5G) and decreased mRNA expression of AR target genes KLK3 and TMPRSS2 (Figure 5H). Contrariwise, overexpressing POM121 in 22Rv1 cells induced a higher accumulation of AR in the nucleus and increased expression of its target genes KLK3 and TMPRSS2 (Figures S5C and S5D). The effect of POM121 on AR signaling, was confirmed in POM121-depleted androgen-sensitive LNCaP cells, in which AR accumulation in the nucleus (Figure S5E) and transcription of AR target genes (Figure S5F) was significantly reduced. Collectively, these results suggest that POM121 regulates AR signaling by enhancing its nuclear localization in PC cells.

A GATA2-POM121 Regulatory Feedback Regulates Aggressiveness in Lethal PC

We next investigated for potential upstream regulators of POM121, selecting as our candidate the transcription factor GATA2, which has recently been reported by us and others as a master regulator that confers aggressiveness in PC cells by enhancing AR signaling and regulating a subset of relevant cancer progressiongenes that include*POM121*(Rodriguez-Bravo et al., 2017; Vidal et al., 2015). We first confirmed this previous observation by assessing that GATA2 knockdown results in POM121 mRNA (Figure 6A) and protein decrease (Figure 6B), and POM121 overexpression partially rescues GATA2 knockdown effects on tumorigenicity (Figure S6A) and survival to standard therapy (Figure S6B). After examining that the *POM121* promoter contained three canonical GATA2-binding elements (GBEs), which we termed GBE1, GBE2, and GBE3 (Figure 6C), we observed that GATA2 directly regulates POM121 expression by binding to its promoter. Chromatin immunoprecipitation followed by qPCR (ChIP-qPCR) assays revealed that GATA2 occupies the three GBEs but not adjacent control regions in the two aggressive PC cell models(Figure 6D).Inaddition,cotransfection assays showed that while GATA2 expression could activate luciferase transcription from a *POM121* promoter reporter, mutation of the GBEs significantly reduced this effect (Figure 6E).

Moreover, because GSEA showed that the POM121 gene signature was significantly enriched in GATA2 signaling genes (Figure 6F), we decided to explore if GATA2 activity was regulated by POM121. We observed that POM121 depletion decreases GATA2 nuclear accumulation (Figure 6G), and GATA2 binds to importin β (Figure S6C), thus suggesting the existence of a positive regulatory feedback loop between POM121 and GATA2 in which GATA2 regulates POM121 transcriptional expression, and in turn, *POM121* regulates GATA2 activity by enhancing its nuclear localization (Figure 6H).

A consequence of our hypothesis that GATA2 transcriptionally upregulates *POM121* is that these genes are co-expressed in clinical prostate cancer tissues. Indeed, a positive correlation

between *GATA2* and *POM121* mRN A levels was observed (Figure 6I) in three prostate cancer public available databases (Barbierietal., 2012; Grasso et al., 2012; Robinson et al., 2015). Immuno his to chemistry analysis with our cohort of human paraffin-embedded PC tissues confirmed this result (Figure 6J), where GATA2 and POM121 protein expression were significantly co-expressed in PC samples. Altogether, these results support the existence of a GATA2-POM121-positive regulatory feedback in PC.

Targeting the POM121-Importin β Signaling Axis Decreases the Growth and Survival of Lethal PC Preclinical Models

Having uncovered that POM121 mediates its effects through its interaction with importin β, we next looked forward for therapeutic opportunities and decided to target the import axis using the pharmacologic importin b inhibitor Importazole (Soderholm et al., 2011) and by genetic knockdown of importin β (Figure S7A). In both cases, we observed a decrease in tumorigenicity (Figures 7A and S7B), proliferation (Figures 7B and S7C) and survival to standard therapy (Figures 7C and S7D) of PC cells. Concurrently, nuclear-cytoplasm fractionation studies showed that Importazole decreased MYC, E2F1, GATA2, and AR nuclear localization (Figure 7D), mimicking the effects previously observed with POM121 depletion. We then tested the *in vivo* efficacy of Importazole in 22Rv1-DR-luciferase labeled and two patient-derived lethal PC (LPC#1 and LPC#2) xenograft models. Importazole treatment of mice bearing 22Rv1-DR-luciferase xenografts showed reduced tumor photon flux (Figure 7E) and tumor weight (Figure 7F). Remarkably, pharmacodynamic studies demonstrated that Importazole efficacy was paralleled by a decrease in the proliferation marker Ki67 (Figure S7E) and reduced nuclear localization of E2F1, MYC, GATA2, and AR in treated xenografts (Figure S7F). Moreover, to assess the combined efficacy of importin b inhibition with standard chemotherapeutic drugs, we treated mice bearing 22Rv1-DR, LPC#1 and LPC#2 xenografts with Importazole together with docetaxel or mitoxantrone and observed a significant decrease in tumor weight (Figure S7G) and increased cleaved caspase 3 expression in xenografts treated with either combination (Figure 7G). Importantly, the overall survival of mice intracardially injected with 22Rv1-DR, LPC#1, and LPC#2 cells significantly increased when treated with Importazole alone and with combined treatment (Figure 7H) without increasing general toxicity (Figure S7H).

DISCUSSION

Advanced carcinomas, including PC, remain lethal diseases with poor prognosis and unsatisfactory clinical outcomes, which provides a rational to further our understanding regarding their underlying pathogenesis. Our research focuses in the study of the NPC and the Nups from which it is composed to unveil their functional relationship with the aggressiveness of advanced PC. Previous studies have already linked specific Nups to tumor formation and progression as drivers of kinase activity by identifying Nups in a wide range of chromosomal translocations that constitutively activate kinases (Chow et al., 2012; Ko¨ hler and Hurt, 2010; Simon and Rout, 2014). However, despite evidence suggesting that some Nups are in fact deregulated in a range of tumor types (Chow et al., 2012; Ko¨ hler and Hurt, 2010; Simon and Rout, 2014), the mechanism by which the NPC may enhance tumor aggressiveness remains a major challenge yet to overcome.

Through comprehensive computational studies using patient datasets and aggressive PC cell models, we identified a significant upregulation in the gene and protein expression of POM121 throughout the development of aggressive PC cells and into their advanced lethal stages, which correlated with effects in tumorigenesis, proliferation, and survival of PC cells that could be reversed through its genetic knockdown. In an attempt to uncover whether the functional effects of POM121 upregulation could be linked with structural changes in the NE, we observed an increase in the number of pores in cells where POM121 was overexpressed, including samples from advanced PC tumors. Notably, POM121 depletion did not alter the structure of pores, suggesting that POM121 may be sufficient but not essential for pore formation in PC cells. Moreover, using genetic and nuclear transport reporter approaches we found that another fundamental mechanism by which POM121 exerted its impact in PC was through a modulation of importin b-mediated nuclear import of specific oncogenic (MYC and E2F1) and PC-related transcription factors (AR and GATA2).

In particular, we demonstrated that an interaction between this Nup and nuclear import receptor importin β exists and that it regulates MYC and E2F1 signaling activity, well-known contributors to PC aggressiveness (Ellwood-Yen et al., 2003; Hawksworth et al., 2010; Liang et al., 2016; Thompson et al., 1989; Zheng et al., 2009), with effects on the tumorigenesis, proliferation, and survival of PC cells. Our data also showcases an enhancing effect of POM121 over AR signaling, which has been extensively linked with the pathogenesis and cell growth of PC during all stages of disease (Knudsen and Penning, 2010; Zong and Goldstein, 2013). Regarding GATA2, our results point to a regulatory loop wherein this transcription factor regulates *POM121* transcriptional expression and, in turn, POM121 regulates GATA2 signaling activity by assisting in its nuclear localization. These results are in congruence with previous studies conducted by our group that identified the role of GATA2 as a master regulator of PC aggressiveness in both an AR-dependent and AR-independent manner (Rodriguez-Bravo et al., 2017; Vidal et al., 2015). It is of interest to note that our findings reveal that GATA2 does not only regulate AR signaling by its pioneer function of enabling AR binding to DNA, but also by indirectly enhancing AR transport into the nucleus through POM121. Importantly, POM121 nuclear import regulation of these transcription factors is specific, because in POM121 gain and loss-of-function studies the nuclear localization of other transcription factors that are transported into the nucleus independently from importins, such as β catenin (Jamieson et al., 2014), remains unaltered. Moreover, POM121 exerts its import function via direct binding to importins. Taken together, our data regarding POM121-importin β-mediated nuclear import of specific transcription factors sets the stage for the unraveling of potential scenarios in which the enhanced import of a given transcription factor may be dependent on its context (i.e., disease stage) and its abundance in a particular cell. Based on this, one is left to wonder whether other NPC-regulated mechanisms, such as chromatin organization, genome integrity, or transcription regulation could be related to the contribution of specific Nups to the lethality of PC. In this regard, a variant of POM121, named soluble POM121 based on its lack of transmembrane domain and association with the NPC, has been recently identified to regulate transcription (Franks et al., 2016). Soluble POM121 binds additional Nups to control transcription at gene promoters in human cells. The contribution of this POM121

variant to cancer remains unknown and forthcoming studies will be necessary to uncover its role.

The POM121-importin β axis described in this study was proved to be pharmacologically targetable through the use of importin β inhibitor Importazole. Either as a single agent or in dual combination with standard-of-care therapy, this inhibitor improved the survival of PC pre-clinical models. The results of such inhibition were concordant with direct targeting of importin β through genetic knockdown and were replicated in patientderived PC models. Importin β targeting reduced the nuclear localization of oncogenic factors E2F1 and MYC, as well as of AR and GATA2, and showed a marked decrease in tumorigenicity, proliferation, and survival to standard care therapy of PC cells. These findings provide proof of concept that targeting nuclear import is a potentially effective therapeutic approach to lethal PC, and thus pave the way for future studies that may further characterize and translate the application of nuclear import inhibitors into cancer treatment.

In summary, our studies shed insight into the prominent role that POM121 exerts in driving aggressiveness in PC lethal stages through its direct interaction with importin β and thus delineate a sequence of molecular events that can be pharmacologically targeted as a feasible therapeutic approach. Our work therefore evidences the major mechanistic role that the NPC plays in cancer pathogenesis and opens the door to future investigations that may be extended to other Nups or extrapolated to other tumor types to broaden our understanding of the NPC involvement in cancer cell biology and oncology as a whole.

STAR★METHODS

KEY RESOURCES TABLE

REAGENT or RESOURCE	SOURCE	IDENTIFIER
Antibodies		
Rabbit polyclonal anti-POM121	GeneTex	GTX102128; RRID: AB_10732546
Rabbit polyclonal anti-NUP62	GeneTex	GTX107973; RRID: AB_1951041
Rabbit polyclonal anti-GATA2	Sigma-Aldrich	HPA005633; RRID: AB_1078954
Mouse monoclonal anti- hnRNP-A1	Sigma-Aldrich	R-4528; RRID: AB_261962
Mouse monoclonal anti-ß-Actin	Sigma-Aldrich	A-5441; RRID: AB_476744
Mouse monoclonal anti-Mab414	Abcam	ab24609; RRID: AB_448181
Rabbit polyclonal anti-TPR	Abcam	ab84516; RRID: AB_1861454
Rabbit polyclonal anti-NUP153	Abcam	ab84872; RRID: AB_1859766
Rabbit polyclonal anti-Lamin A	Abcam	ab26300; RRID: AB_775965
Rabbit monoclonal anti-c MYC	Abcam	ab32072; RRID: AB_731658
Rabbit monoclonal anti-E2F1	Abcam	ab179445
Mouse monoclonal anti-fluorescent protein (GFP)	Santa Cruz Biotechnology	SC-9996; RRID: AB_627695
Rabbit polyclonal anti-karyopherin ß1 (H-300)	Santa Cruz Biotechnology	SC-11367; RRID: AB_2265549
Mouse monoclonal anti-karyopherin a2 (B-9)	Santa Cruz Biotechnology	SC-55538; RRID: AB_831493
Rabbit polyclonal anti-androgen receptor (N-20)	Santa Cruz Biotechnology	SC-816; RRID: AB_1563391
Mouse monoclonal anti-Tubulin a (DM1A)	Millipore	CP06; RRID: AB_2617116
Rabbit polyclonal anti-cleaved caspase-3	Cell Signaling	9661S; RRID: AB_2341188
Mouse monoclonal anti-ß-catenin	Invitrogen	13–8400; RRID: AB_2533039
Anti-mouse IgG, Horseradish Peroxidase	GE	NA931; RRID: AB_772210
Anti-Rabbit IgG, Horseradish Peroxidase	GE	NA934; RRID: AB_2722659
Alexa Fluor 488 AffiniPure Donkey anti-Mouse IgG (H+L)	Jackson ImmunoResearch	715–545-150; RRID: AB_2340846
Rhodamine (TRITC) AffiniPure Donkey anti-Rabbit IgG (H+L)	Jackson ImmunoResearch	711–025-152; RRID: AB_2340588
Rabbit polyclonal GATA2 (H-116)	Santa Cruz	sc-9008; RRID: AB_2294456
Rabbit polyclonal IgG Control (Chip grade)	Abcam	ab171870; RRID: AB_2687657
Goat anti rabbit IgG with 10 nm AuNP	Electron Microscopy Sciences	25108
Bacterial and Virus Strains		
NEB 5-alpha competent E. coli	New England BioLabs	2987H
Biological Samples		
Prostate cancer paraffin embedded tumor samples	Thomas Jefferson University GU Biorepository	See STAR Methods
Prostate cancer paraffin embedded tumor samples	Mount Sinai GU Biorepository	See STAR Methods
Chemicals, Peptides, and Recombinant Proteins		
Docetaxel	Selleck Chemicals	S1148
Cabazitaxel	Selleck Chemicals	S3022

REAGENT or RESOURCE	SOURCE	IDENTIFIER
Mitoxantrone	Selleck Chemicals	S2485
Importazole	Selleck Chemicals	S8446
Selinexor	Selleck Chemicals	S7252
Matrigel	Corning	354230
Crystal violet	Acros Organics	229641000
Difco Noble Agar	BD Biosciences	214230
Dynabeads Protein G	Invitrogen	10004D
Dynabeads Protein A	Invitrogen	10002D
XeneLight D-Luciferin Potassium Salt	PerkinElmer	122799
Critical Commercial Assays		
RNeasy Mini kit	QIAGEN	74106
SuperScript III First-Strand Synthesis SuperMix Kit	Thermo Scientific	18080400
NE-PER Nuclear and Cytoplasm Extraction Reagents	Thermo Scientific	78833
Dual-Luciferase-Assay System	Promega	E1910
TruSeq ChIP Library Preparation Kit	Illumina	IP-202–1012
Deposited Data		
RNA-seq raw data of POM121-knockdown	This paper	GEO: GSE103637
RNA-seq raw data of GATA2-knockdown	Vidal etal., 2015	GEO: GSE58966
Transcriptome of prostate cancer patient samples	Grasso et al., 2012	GEO: GSE35988
Transcriptome of prostate cancer patient samples	Robinson et al., 2015	dbGap: phs000915.v1.p1.
Transcriptome of prostate cancer patient samples	Barbieri et al., 2012	dbGaP: phs000447.v1.p1
Experimental Models: Cell Lines		
DU145	ATCC	ATCC HTB-81
22Rv1	ATCC	ATCC CRL-2505
LNCaP	ATCC	ATCC CRL-1740
HEK293	ATCC	ATCC CRL-1573
DU145-DR	Domingo-Domenech et al., 2012; Mohr et al., 2017	N/A
22Rv1 -DR	Domingo-Domenech et al., 2012; Mohr et al., 2017	N/A
LPC#1	Vidal et al., 2015; Williams et al., 2015	N/A
LPC#2	Vidal et al., 2015; Williams et al., 2015	N/A
Experimental Models: Organisms/Strains		
NOD.Cg-Prkdc^{scid} IL2rg^{tm1Wjl} (NSG) mice	Jackson mice	005557
Oligonucleotides		
siRNA Control#1	Ambion	AM4636

REAGENT or RESOURCE	SOURCE	IDENTIFIER
siRNA POM121 #1	Life Technologies	s59623
siRNA POM121#2	Life Technologies	s19145
siRNA NUP188#1	Life Technologies	s23964
siRNA NUP188#2	Life Technologies	s23966
siRNA NUP210#1	Life Technologies	s23331
siRNA NUP210#2	Life Technologies	s23332
siRNA NUP85#1	Life Technologies	s36610
siRNA NUP85#2	Life Technologies	s36611
siRNA NUP62#1	Life Technologies	s24247
siRNA NUP62#2	Life Technologies	s24248
siRNA NUP214#1	Life Technologies	s15547
siRNA NUP214#2	Life Technologies	s15549
siRNA TPR#1	Life Technologies	s14353
siRNA TPR#2	Life Technologies	s14354
shRNA POM121.486	This paper	N/A
shRNA POM121.834	This paper	N/A
shRNA non-targeting Renilla control	This paper	N/A
Primers for POM121 RT-PCR	This paper	N/A
Forward ACATTCCCTTTGGCTCAA		
Reverse CAGCCGGGGCTGCAGAGT		
Primers for NUP188 RT-PCR	This paper	N/A
Forward ACATTGGCGGCGATTGTTAGA		
Reverse GCTGATTCTTAAACCCAGTTCCT		
Primers for NUP210 RT-PCR	This paper	N/A
Forward TGGTCTTCGAGTGGACGATTG		
Reverse GCAGGGCGTACATTCTTGTAG		
Primers for NUP85 RT-PCR	This paper	N/A
Forward GGCGAGCCAACAGTCACTTT		
Reverse ACTCTTCGTCAATTCTCTGGAGG		
Primers for NUP62 RT-PCR	This paper	N/A
Forward GGAACAGCGACTCTTGCTTC		
Reverse GGTGCTCGATATGGCATTAGTG		
Primers for NUP214 RT-PCR	This paper	N/A
Forward TGACTCCCCTGAGGAATTGC		
Reverse GCGAAGACCAGACCATATTTGTT		
Primers for TPR RT-PCR	This paper	N/A
Forward AACGCCAGCGTGAGGAATATG		
Reverse ATTACGTGGTTACCCCTTGCT		
Primers for POM121 GBE1 mutant cloning	This paper	N/A

REAGENT or RESOURCE	SOURCE	IDENTIFIER
Forward CAGCTTTATTAAggggTAATTCACATACCA TGC Reverse GCATGGTATGTGAATTAccccTTAATAAAG CTG		
Primers for POM121 GBE2 mutant cloning	This paper	N/A
Forward CAAAATCCACCCggggTCTGGGCCATG Reverse CATGGCCCAGAccccGGGTGGATTTTG		
Primers for POM121 GBE3 mutant cloning	This paper	N/A
Forward GTGCACGCTGGggggTTTAAGTCTCC		
Reverse GGAGACTTAAAccccCCAGCGTGCAC		
Primers for POM121 GBE1 ChIP q-PCR	This paper	N/A
Forward TGAATGGCTGAGGAAACTGA		
Reverse TAGGGCTAGGGAGTGGGTTT		
Primers for POM121 GBE2 ChIP q-PCR	This paper	N/A
Forward CCTAGCCCTAGGCAACCACT		
Reverse CTCCAGCACAGCCTGTTACC		
Primers for POM121 GBE3 ChIP q-PCR	This paper	N/A
Forward TTCCAAACCAGTTGGGTCTC		
Reverse GTCCCTGACACTCGCTATGG		
Primers for Negative control ChIP q-PCR	This paper	N/A
Forward TGCATCCATATTTTGCAGGA		
Reverse GAATGATTGGCCCGTAGAGA		
Recombinant DNA		
rtTA3-IRES-EcoR-Puro (RIEP2)	gift from Dr. Scott Lowe	N/A
TRIN-E vector	gift from Dr. Scott Lowe	N/A
pET30a GST-POM121 WT (266–700)	This paper (Genescript)	N/A
pET30a GST-POM121 ANPC (510–700)	This paper (Genescript)	N/A
Human 6 × His-Importin ß1	Novoprotein	CP58
Human 6 × His-Importin a2	Novoprotein	CE62
pET28-MBP POM121 NLS (291–320) wild type (wt)	Kralt et al., 2015	N/A
pET28-MBP POM121 NLS (291–320) mutant (mut) bearing K313A and K295A mutations in critical residues of major and minor NLS binding sites	Kralt et al., 2015	N/A
pGEX-6P-1 Importin a1	Kralt et al., 2015	N/A
pQE60 Importin ß1	Mitrousis et al., 2008	N/A
pEGFP-N1 POM121 siRNA resistant full length	This paper	N/A
pEGFP-N1 POM121 siRNA resistant POM121 mutant unable to localize to the NPC and bind to Importins lacking amino acids 1–509 (referred as DNPC)	This paper	N/A

REAGENT or RESOURCE	SOURCE	IDENTIFIER
Rev-GR-GFP retroviral vector	Rodriguez-Bravo et al., 2014	N/A
GFP tagged NUP62	Genscript	clone ID OHu26446, NM_153719.3 ORF
pGL4.10 reporter	Promega	E6651
pGL4.10 POM121 promoter	This paper	N/A
pGL4.10 POM121 Promoter GBE1 mutant	This paper	N/A
pGL4.10 POM121 Promoter GBE2 mutant	This paper	N/A
pGL4.10 POM121 Promoter GBE3 mutant	This paper	N/A
pRL- Renilla Luciferase Control Reporter Vector	Promega	E2231
pCMV-GATA2	Vidal etal., 2015	N/A
Software and Algorithms		
Prism	GraphPad	https://www.graphpad.com/scientific-software/prism/
Living Image software v.4.2	PerkinElmer	http://www.perkinelmer.com
SPSS	IBM Analytics	https://www.ibm.com/analytics/spss-statistics-software
GSEA Molecular Signature Database	Broad Institute	https://www.broadinstitute.org/msigdb
DAVID Bioinformatics Resources	David Bioinformatics	https://david.ncifcrf.gov/

CONTACT FOR REAGENT AND RESOURCE SHARING

Further information and requests for reagents should be directed to and will be fulfilled by the Lead Contact, Josep Domingo-Domenech (josep.domingo-domenech@jefferson.edu).

EXPERIMENTAL MODEL AND SUBJECT DETAILS

Human PC tissues

Human formalin fixed paraffin embedded primary (n = 56) and advanced metastatic PC (n = 68) tissue samples were collected from the Sidney Kimmel Cancer Center at Jefferson University GU Biorepository (IRB#13D.507) and Mount Sinai GU Biorepository (IRB#11–01565) under an Institutional Review Board approved protocol. All patients provided written informed consent to obtain tumor biopsies. All tissue sections were reviewed by a pathologist to confirm PC origin.

Animal experimental models

All animal experiments were performed in the AAALAC-accredited Comparative Bioscience Center at Thomas Jefferson University and Mount Sinai School of Medicine. Experiments were in accordance with NIH guidelines for Animal Care and Use, approved and overseen by Thomas Jefferson and Mount Sinai Universities Institutional Animal Care and Use Committee. All mouse procedures were performed with NOD.Cg-Prkdc^{scid} IL2rg^{tm1Wjl} (NSG) female mice obtained from Jackson Laboratories. For intracardiac injections, 3–4 weeks old mice were used. For the rest of the experiments 6–7 weeks old mice were used. See Method Details for mice work specific procedures.

PC cells and PC preclinical patient derived xenograft models

Prostate cancer DU145, 22Rv1, and LNCaP cells, and HEK293 cells were obtained from ATCC. Aggressive castration-resistant and chemotherapy resistant PC cells, DU145-DR and 22Rv1-DR, were generated as previously described by our group (DomingoDomenech et al., 2012; Mohr et al., 2017). Briefly, Docetaxel-Resistant cells, DU145-DR and 22Rv1-DR, were generated by culturing cells with vehicle (DMSO) and docetaxel in a dose-escalation manner using 72 hours exposures. After several passages docetaxel resistant phenotype was confirmed by colony formation assays and q-PCR of selected genes (Mohr et al., 2017). PC cells were maintained in RPMI media (GIBCO) and HEK293 cells in DMEM (GIBCO) media, both supplemented with 10% FBS and 1% penicillin/streptomycin (GIBCO). Cells were grown at 37°C in a humidified atmosphere with 5% CO_2. Two advanced aggressive PC xenograft models (LPC#1 and LPC#2) generated from circulating tumor cells from PC patients previously characterized by our group (Vidal et al., 2015; Williams et al., 2015) were used in experiments to test the in vivo activity of Importin b inhibitor, Importazole alone and in combination with standard-of-care therapy.

METHOD DETAILS

Focused loss-of-function genetic screen of clinically upregulated Nups

Custom siRNAs against 7 clinically upregulated nucleoporins were obtained from life technologies (Silencer Select siRNA). For our screening system, we used the PC cell line models, DU145-DR and 22Rv1-DR which recapitulate the aggressive nature of lethal PC and its molecular landscape. Efficacy of Nup depletion (mRNA decrease > 80%) was tested by conventional quantitative RT-PCR (see methods below) using two independent siRNAs for each Nup. Three functional criteria were used to consider a Nup as a “hit” of PC aggressiveness. First, decrease on tumorigenicity measured by soft agar colony formation assays; second, decrease in cell proliferation measured through population doubling assays; and third, reduced survival measured through colony formation assays by exposing PC cells to standard-of-care therapies, such as the antimitotic agents, docetaxel and cabazitaxel, and the DNA damaging agents, mitoxantrone and radiotherapy.

RNA extraction and qRT-PCR

RNA was isolated using the RNeasy Mini kit (QIAGEN) in accordance with manufacturer’s instructions. Complementary DNA was synthesized from equivalent concentrations of total RNA using the SuperScript III First-Strand Synthesis SuperMix Kit (Invitrogen) in accordance with manufacturer’s instructions. Amplification was carried out using a Mastercycler ep realplex (Eppendorf). Cycle threshold values were determined and normalized to the loading control for each experiment. Fold changes for experimental groups relative to respective controls were calculated using MX Pro software (Agilent Technologies).

Bioinformatics data analysis

Transcriptome profiles of primary (n = 59) and warm autopsy (n = 35) PC tissues were obtained from NCBI Gene Expression Omnibus database (GSE35988) (Grasso et al., 2012).

Differentially expressed genes between experimental conditions were determined by random permutation-based t test with a statistical significance cut-off of false discovery rate (FDR) < 0.05. E2F1 and MYC target gene signatures were obtained from literature (Bild et al., 2006; Coller et al., 2000; Dang et al., 2006; Ishida et al., 2001; Ren et al., 2002; Schuhmacher et al., 2001; Yu and Thomas-Tikhonenko, 2002) (Table S5). GATA2 target gene signature (GSE58966) was derived from our previous publication (Vidal et al., 2015). Modulation of molecular pathway gene sets and target gene signatures from Molecular Signature Database (MSigDB, https://www.broadinstitute.org/msigdb) was determined by using a modified version of Gene Set Enrichment Analysis (Nakagawa et al., 2016) and DAVID Bioinformatics Resources (https://david.ncifcrf.gov/) with a statistical significance cut-off of FDR < 0.05. Spearman correlation analysis between POM121 and GATA2 mRNA expression was performed in three publicly available databases containing transcriptomic data from PC tissue samples (Accession numbers GSE35988; dbGaP; phs000447.v1.p1, and dbGap: phs000915.v1.p1).

Transcriptome profiling of POM121-knockdown cells

To characterize the transcriptional program regulated by POM121, we performed RNA sequencing of PC models, DU145-DR and 22Rv1-DR, after 72 hours of being transfected with siControl, and two siRNAs targeting POM121 (biological replicates of n = 3 for each condition). High-quality total RNA samples (RNA Integrity score > 7.7 by Agilent Bioanalyzer) were subjected to poly A-selected sequencing library preparation using TruSeq RNA Sample Prep Kit ver.2 (Illumina) following manufacturer's protocol. The libraries were sequenced by HiSeq 2500 genome sequencer (Illumina) to generate 100 bp single-end reads. Data preprocessing and transcript abundance calculation (FPKM: fragments per kilo bases of exons for million mapped reads) were performed using TopHat and Cufflinks software using the human reference genome (hg19).

Immunohistochemistry

Immunohistochemistry analyses were conducted on PC formalin fixed paraffin embedded tissue sections from human samples and cell line (22Rv1-DR) or lethal PC (LPC) xenografts. Tissue sections (5 mm) were deparaffinized and submitted to standard peroxidasebased immunohistochemistry procedures. Quantification of positive cells was determined by counting the number of tumor cells in 10 contiguous high power fields in three different areas of each section, and referred to the total number of counted cancer cells. GATA2 and POM121 protein co-expression was analyzed in PC formalin fixed paraffin embedded tissue samples. Samples where scored as POM121 or GATA2 "low" when negative staining or < 50% PC cells with weak nuclear staining and "high" when ≥ 50% of PC cells displayed a strong intensity nuclear staining in 4 contiguous high power fields in three different areas of each section.

High resolution electron microscopy imaging

All electron microscopy studies were done on a H7650 (Hitachi) electron microscope. For cellular and nuclear pore complex morphological studies PC cells and tissues were fixed with 3% glutaraldehyde with 0.2M sodium cacodylate buffered at pH 7.4. Fixation with 4% Paraformaldehyde in PBS buffer for 1 hour and maintained in PBS was used for POM121

immunogold staining of PC tissues. Briefly, POM121 immunogold staining was performed as follows. First, tissue was processed and embedded in LR White and polymerized at –20°C with UV light. Next, ultrathin sections from the tissue blocks were cut and subjected to the following immunostaining protocol: sections were treated with ammonium chloride for 15 minutes to block any free aldehyde groups. After extensive washing with PBS treated with whole goat serum (1:50 dilution in PBS) for 15 min to block any non-specific binding sites, washed with PBS and incubate with primary antibody (POM121 GeneTex, 1:20 dilution) overnight at room temperature. Next day samples were washed, incubated with secondary antibody (goat anti rabbit IgG with 10 nm AuNP 1:25 dilution in PBS obtained from Electron Microscopy Sciences) for 3–4 hours at room temperature, washed with PBS, fixed with 3% glutaraldehyde, washed with distilled water and counter stained with uranyl acetate.

Soft agar colony formation assays

Tumorigenic capacity of PC cells was assessed *in vitro* by plating 10^3 cells in a 0.3% agar solution on top of a 0.6% agar layer in 35mm culture dishes. Cells were cultured with RPM1 media containing 10% FBS and 1% penicillin/streptomycin. After 14–21 days colonies were counted microscopically.

Cell population doubling assays

Proliferation capacity of PC cells were performed by plating 10^4 cells in 35mm culture dishes and counting the number of cells at indicated time points using an automated cell counter (Countess II Life Technologies).

Colony formation assays

Clonogenic assays in response to drug treatment were performed by plating 10^3 cells in 35mm culture dishes. After 24 hours cells were treated with vehicle controls or with drugs for 72 hours. After 10–14 days cell culture dishes were washed with PBS, stained with a 2% crystal violet 10% formalin solution and formed colonies counted macroscopically.

Inducible POM121 shRNAs

For inducible shRNA mediated inhibition of POM121, two clones (POM121.486 and POM121.834) and a non-targeting Renilla control were selected following the screen of a custom library. Predictions of shRNA were obtained using “sensor rules” to enrich for predictions harboring sequence features associated with effective shRNAmir processing and potent knockdown (Fellmann et al., 2011). DU145-DR and 22Rv1-DR cells were initially infected with a lentivirus containing a reverse tetracycline-controlled trans-activator 3 (rtTA3)-IRES-EcoR-Puro (RIEP2) and selected with puromycin (2 μg/ml) to generate stable cells. Subsequently, cells were infected with retroviruses containing a TRIN-E vector with the control or POM121-targeting shRNAs and selected with neomycin (0.4 mg/ml). POM121 depletion efficiency was evaluated by immunoblotting 72 hours after the addition of doxycycline (1 μg/ml) to culture media. RIEP2 and TRIN-E vectors were a generous gift from Dr. Scott Lowe (Memorial Sloan Kettering Cancer Center, NY, USA). Studies with stably expressing shRNA sublines were performed with pools passage no more than five times.

Tumorigenic capacity

Cancer cells were implanted subcutaneously in a 1:1 mixture of growth medium and Matrigel (Corning) at different dilutions (10, 100 and 1,000 cells). Tumor incidence (number of tumors/number of injections) and tumor latency (time from injection to first tumor palpability) were evaluated weekly. Tumors formed were confirmed histologically. When tumors became palpable at a single injection site, they were surgically removed to allow continued evaluation of other sites. Mice were monitored for up to 6 months, and animals with no sign of tumor formation were examined at necropsy for confirmation.

Monitoring of subcutaneous xenograft growth

For *in vivo* studies involving shRNAs against POM121 and Importazole, subcutaneous xenografts were generated by implantation of 10^6 indicated PC cells in a 1:1 mixture of culture medium RPMI (GIBCO) and Matrigel (Corning) into the flanks of NSG mice. When subcutaneous tumors became palpable, mice were randomly assigned to treatment groups containing four animals. The vehicles for chemotherapy and Importazole were 10% DMSO in sterile 1xPBS. Tumor dimensions were monitored weekly using Vernier calipers. Tumor volume was calculated according to the formula $V = (a^2xb)/2$ where a and b are the minimal and maximal diameter in millimeters, respectively. In accordance with institutional guidelines, mice bearing subcutaneous xenografts greater than $500mm^3$ were sacrificed. Explanted tumors were weighed, formalin fixed, and embedded in paraffin for pathological analysis.

Immunofluorescence microscopy and cell imaging analysis

For immunofluorescence microscopy, cells on coverslips were fixed and permeabilized with 4% paraformaldehyde and 0.2% Triton X-100. Three percent BSA was used as the blocking and antibody dilution buffer. After mounting in Prolong Gold (Invitrogen), samples were imaged on a Zeiss LSM 510 META or Zeiss LSM 710 axiovert confocal microscope using a 63× Plan-Neofluar 1.4 NA oil immersion objective lens (Carl Zeiss, Germany). In the nuclear transport assay, nuclear/cytoplasmic ratios were quantified in PC cells stably expressing a glucocorticoid receptor (GR)-GFP reporter (Rodriguez-Bravo et al., 2014) after 15 minutes exposure to dexamethasone (1μM) in different experimental conditions. Nuclear export of PC cells was inhibited with the XPO-1 inhibitor Selexinor (1mM) 2 hours prior exposing cells to dexamethasone. GR-GFP was visualized using a GFP antibody (Santa Cruz Biotechnology). Images were quantified using ImageJ (NIH) and the mean pixel intensity/μm was determined to generate the nuclear/cytoplasmic ratios.

Immunoblot and immunoprecipitation

Whole cell extracts were prepared in sample buffer and analyzed by immunoblot using standard procedures. For immunoprecipitation, extracts were incubated with the indicated antibodies overnight at 4C. Following 2 hours incubation with protein A/G Dynabeads (Invitrogen), beads were washed four times, resuspended in 1× Laemmli sample buffer and boiled for 5 minutes. Subcellular nuclear cytoplasm protein fractionation was performed using the NE-PER Nuclear and Cytoplasm Extraction Reagents (Thermo Scientific) following the protocol supplied by the manufacturer. SDS-PAGE resolved proteins were

transferred to nitrocellulose membranes and incubated with primary antibodies. Secondary antibodies were used at 1:5000.

Recombinant Protein Expression and Pull-Down Assays

GST-tagged POM121^{wt} (266–700) and POM121$^{\Delta NPC}$ (510–700) were synthesized and cloned into vector pET30a for protein expression in E. coli (Genescript). Human 6 3 His-Importin β1 and 6 × His-Importin α2 were obtained from Novoprotein (Cat# CP58 and CE62). POM121 NLS (291–320) wild-type (wt) and mutant (mut) (bearing K313A and K295A mutations in critical residues of major and minor NLS binding sites) cloned in pET28-MBP (Kralt et al., 2015) and Importin α1 and β1 cloned in pGEX-6P-1 (GE Healthcare) and pQE60 (QIAGEN) respectively (Kralt et al., 2015; Mitrousis et al., 2008), were expressed in *E. coli* and purified as previously described. For GST tag pull-down assays, human GST-POM121 proteins or GST alone were loaded onto Glutathione Sepharose 4B affinity chromatography resin (GE) in Binding Buffer (20 mM Tris-Cl, pH 7.4, 150 mM NaCl, 1 mM EGTA, 0.1% Tween 20, 1 mM DTT). After 1 hour incubation with human 6 × His-Importin a2 and b1, beads were washed and eluted in 1 × Laemmli sample buffer. For His-tag pull-down assays, human 6 × His-Importin α2 and β1 proteins were loaded onto HisPur isolation Ni-NTA magnetic beads (Thermo Scientific) in Binding Buffer. After 1 hour incubation with human GST-tagged POM121 WT or DNPC, beads were washed and eluted in 1 × Laemmli sample buffer. For MBP-tag pull-down assays MBP-POM121 NLS WT or mutant proteins were loaded onto Amylose magnetic beads in Binding Buffer. After 1 hour incubation with Importin a1 and b1, beads were washed and eluted in 1× Laemmli sample buffer. All samples were resolved by 10% SDS-PAGE and visualized by Coomassie Brilliant Blue staining and Western Blotting.

Molecular cloning

POM121 siRNA resistant full length (1–1249 amino acids) POM121 (POM121^{wt}) and a POM121 mutant unable to localize to the NPC and bind to Importins lacking amino acids 1–509 (referred as ΔNPC) were synthesized using GeneArt Gene Synthesis (Thermo Fisher Scientific) and subsequently sub cloned into the pEGFP-N1 expressing vector (Clontech) via NheI-BamHI restriction digest. A previously reported import reporter retroviral vector containing an HIV-1 Rev-glucocorticoid receptor-GFP fusion (Rodriguez-Bravo et al., 2014) was used to generate virus and transduce target cells to generate stably expressing cell lines after neomycin (0.4 mg/ml) selection. GFP tagged NUP62 mammalian expression plasmid was obtained from Genscript (clone ID OHu26446, NM_153719.3 ORF) and transfected into PC cells. The *POM121* promoter sequence (–1000 to +400 nucleotides) was amplified by PCR and cloned into the pGL4.10 reporter vector using NheI and XhoI sites (Promega). The resulting vector was used as template to mutate GATA2 binding sequences by site directed mutagenesis. After synthesizing the mutant strand by PCR, template sequence was digested with *DpnI* restriction enzyme for 2 hours at 37°C. The mutant vector was transformed into competent cells for nick repair, plasmid DNA was recovered and mutation of the binding site was confirmed by Sanger sequencing.

Chromatin immunoprecipitation

Chromatin from crosslinked DU145-DR and 22Rv1-DR cells was sonicated, pre-cleared and incubated overnight with 3μg of the corresponded antibody in RIPA buffer and precipitated with protein G/A-Sepharose. The DNA-protein-antibody complexes were then washed three times with RIPA, three times with RIPA- NaCl, twice with Litium Buffer, and twice with 1× TE. Cross-linkage of the co-precipitated DNA–protein complexes was reverse and the immunoprecipitated DNA was analyzed by qPCR using the primers listed above.

Luciferase reporter assay

HEK293 cells were seeded into 12- well plates at a density of 1.25×10^5 and allowed to attach overnight. Transfection mix was prepared by combining 198ng of pGL4.10, 19.8ng of pRL-Renilla, and 882ng of a GATA2 expression vector or RFP control. Luciferase activity was measured with Dual-Luciferase-Assay kit (Promega) 48 hours after transfection, mixing 50ml of lysate with 50μl of Luciferase Buffer Assay (Dual Glo, Promega) and analyzed in an automatic luminometer. 50ml of Stop & Glo reagent was then added and Renilla luminescence measured after 10 minutes of incubation. Ratios of Firefly versus Renilla luciferase were calculated to determine promoter activity.

In vivo bioluminescence imaging

Imaging was performed using an IVIS Spectrum (Xenogen) imager. Animals received luciferin at 200mg/kg by intraperitoneal injection 5 minutes prior to imaging. Animals were then anesthetized using an isoflurane vaporizer and placed onto the warmed stage inside the camera box. At this stage animals received continuous exposure to 2% isoflurane. For quantification, rectangular regions of interest (ROIs) incorporating the entire animal were measured. The signal was measured in photons per second using Living Image software v. 4.2 (Xenogen).

Mouse intracardiac injections

Intracardiac injections were performed as previously described (Vidal et al., 2015). Briefly, the ventral thorax of 3–4 weeks old mice were shaved prior anesthesia with an isoflurane vaporizer and nose cone. The thorax was sterilized with iodine and alcohol and a sterile marker was used to mark a location half way between the sternal notch and the xyphoid process. 100μl from a 1×10^6cell/ml suspension of 22Rv1-DR, LPC#1 or LPC#2 cells in sterile 1xPBS was drawn into a 30.5 gauge needle. The upright syringe was gently inserted through the mark and for each injection successful penetration into the left ventricle was confirmed visually by a pulse of bright red blood into the syringe. Following each experiment, a detailed necropsy was performed to grossly and histologically confirm disseminated tumor burden.

General toxicity monitoring

Body weights for every mouse were recorded every three days and fluctuations were computed by the percentage of current body weight relative to baseline. When animals showed signs of weight loss therapy was discontinued. In accordance with institutional guidelines all animals experiencing greater than 20% weight loss were sacrificed.

QUANTIFICATION AND STATISTICAL ANALYSIS

Statistical analysis was carried out with SPSS version 19.0 (SPSS, Inc.). To analyze correlations, we used Spearman's correlation tests when the two variables were assessed as continuous, t test when one variable was assessed as continuous and the other as qualitative and χ^2 test (Fisher exact test) when the two variables were qualitative. In pre-clinical studies, survival analyses were performed using the Kaplan–Meier method and curves were compared by the log rank test. All the statistical tests were conducted at the two-sided 0.05 level of significance.

Supplementary Material

Refer to Web version on PubMed Central for supplementary material.

ACKNOWLEDGMENTS

V.R.-B. is supported by NIH/NCI grant K22 CA207458. A.L. is supported by DoD grants CA150272P2 and CA150178. Y.H. is supported by the NIH/NCI grant R01 DK099558, E.U. ERC-2014-AdG-671231 HEPCIR, and DoD W81XWH-16–1-0363. J.D.-D. is supported by NIH/NCI grant R01 CA207311.

REFERENCES

Antonin W, Franz C, Haselmann U, Antony C, and Mattaj IW (2005). The integral membrane nucleoporin pom121 functionally links nuclear pore complex assembly and nuclear envelope formation. Mol. Cell 17, 83–92. [PubMed: 15629719]

Barbieri CE, Baca SC, Lawrence MS, Demichelis F, Blattner M, Theurillat JP, White TA, Stojanov P, Van Allen E, Stransky N, et al. (2012). Exome sequencing identifies recurrent SPOP, FOXA1 and MED12 mutations in prostate cancer. Nat. Genet 44, 685–689. [PubMed: 22610119]

Beer TM, Armstrong AJ, Rathkopf DE, Loriot Y, Sternberg CN, Higano CS, Iversen P, Bhattacharya S, Carles J, Chowdhury S, et al.; PREVAIL Investigators (2014). Enzalutamide in metastatic prostate cancer before chemotherapy. N. Engl. J. Med 371, 424–433. [PubMed: 24881730]

Bild AH, Yao G, Chang JT, Wang Q, Potti A, Chasse D, Joshi MB, Harpole D, Lancaster JM, Berchuck A, et al. (2006). Oncogenic pathway signatures in human cancers as a guide to targeted therapies. Nature 439, 353–357. [PubMed: 16273092]

Blobel G (1985). Gene gating: a hypothesis. Proc. Natl. Acad. Sci. USA 82, 8527–8529. [PubMed: 3866238]

Brickner DG, and Brickner JH (2012). Interchromosomal clustering of active genes at the nuclear pore complex. Nucleus 3, 487–492. [PubMed: 23099887]

Chow KH, Factor RE, and Ullman KS (2012). The nuclear envelope environment and its cancer connections. Nat. Rev. Cancer 12, 196–209. [PubMed: 22337151]

Coller HA, Grandori C, Tamayo P, Colbert T, Lander ES, Eisenman RN, and Golub TR (2000). Expression analysis with oligonucleotide microarrays reveals that MYC regulates genes involved in growth, cell cycle, signaling, and adhesion. Proc. Natl. Acad. Sci. USA 97, 3260–3265. [PubMed: 10737792]

Cutress ML, Whitaker HC, Mills IG, Stewart M, and Neal DE (2008). Structural basis for the nuclear import of the human androgen receptor. J. Cell Sci 121, 957–968. [PubMed: 18319300]

Dang CV, and Lee WM (1988). Identification of the human c-myc protein nuclear translocation signal. Mol. Cell. Biol 8, 4048–4054. [PubMed: 3054508]

Dang CV, O'Donnell KA, Zeller KI, Nguyen T, Osthus RC, and Li F (2006). The c-Myc target gene network. Semin. Cancer Biol 16, 253–264. [PubMed: 16904903]

de Bono JS, Oudard S, Ozguroglu M, Hansen S, Machiels JP, Kocak I, Gravis G, Bodrogi I, Mackenzie MJ, Shen L, et al.; TROPIC Investigators (2010). Prednisone plus cabazitaxel or

mitoxantrone for metastatic castration-resistant prostate cancer progressing after docetaxel treatment: a randomised open-label trial. Lancet 376, 1147–1154. [PubMed: 20888992]

de Bono JS, Logothetis CJ, Molina A, Fizazi K, North S, Chu L, Chi KN, Jones RJ, Goodman OB, Jr., Saad F, et al.; COU-AA-301 Investigators (2011). Abiraterone and increased survival in metastatic prostate cancer. N. Engl. J. Med 364, 1995–2005. [PubMed: 21612468]

Dey P (2010). Cancer nucleus: morphology and beyond. Diagn. Cytopathol 38, 382–390. [PubMed: 19894267]

Domingo-Domenech J, Vidal SJ, Rodriguez-Bravo V, Castillo-Martin M, Quinn SA, Rodriguez-Barrueco R, Bonal DM, Charytonowicz E, Gladoun N, de la Iglesia-Vicente J, et al. (2012). Suppression of acquired docetaxel resistance in prostate cancer through depletion of notch- and hedgehog-dependent tumor-initiating cells. Cancer Cell 22, 373–388. [PubMed: 22975379]

Doucet CM, Talamas JA, and Hetzer MW (2010). Cell cycle-dependent differences in nuclear pore complex assembly in metazoa. Cell 141, 1030–1041. [PubMed: 20550937]

Ellwood-Yen K, Graeber TG, Wongvipat J, Iruela-Arispe ML, Zhang J, Matusik R, Thomas GV, and Sawyers CL (2003). Myc-driven murine prostate cancer shares molecular features with human prostate tumors. Cancer Cell 4, 223–238. [PubMed: 14522256]

Fellmann C, Zuber J, McJunkin K, Chang K, Malone CD, Dickins RA, Xu Q, Hengartner MO, Elledge SJ, Hannon GJ, and Lowe SW (2011). Functional identification of optimized RNAi triggers using a massively parallel sensor assay. Mol. Cell 41, 733–746. [PubMed: 21353615]

Franks TM, Benner C, Narvaiza I, Marchetto MC, Young JM, Malik HS, Gage FH, and Hetzer MW (2016). Evolution of a transcriptional regulator from a transmembrane nucleoporin. Genes Dev. 30, 1155–1171. [PubMed: 27198230]

Georget V, Lobaccaro JM, Terouanne B, Mangeat P, Nicolas JC, and Sultan C (1997). Trafficking of the androgen receptor in living cells with fused green fluorescent protein-androgen receptor. Mol. Cell. Endocrinol 129, 17–26. [PubMed: 9175625]

Grasso CS, Wu YM, Robinson DR, Cao X, Dhanasekaran SM, Khan AP, Quist MJ, Jing X, Lonigro RJ, Brenner JC, et al. (2012). The mutational landscape of lethal castration-resistant prostate cancer. Nature 487, 239–243. [PubMed: 22722839]

Hallberg E, Wozniak RW, and Blobel G (1993). An integral membrane protein of the pore membrane domain of the nuclear envelope contains a nucleoporin-like region. J. Cell Biol 122, 513–521. [PubMed: 8335683]

Hawksworth D, Ravindranath L, Chen Y, Furusato B, Sesterhenn IA, McLeod DG, Srivastava S, and Petrovics G (2010). Overexpression of C-MYC oncogene in prostate cancer predicts biochemical recurrence. Prostate Cancer Prostatic Dis. 13, 311–315. [PubMed: 20820186]

Ishida S, Huang E, Zuzan H, Spang R, Leone G, West M, and Nevins JR (2001). Role for E2F in control of both DNA replication and mitotic functions as revealed from DNA microarray analysis. Mol. Cell. Biol 21, 4684–4699. [PubMed: 11416145]

Ivanova IA, Vespa A, and Dagnino L (2007). A novel mechanism of E2F1 regulation via nucleocytoplasmic shuttling: determinants of nuclear import and export. Cell Cycle 6, 2186–2195. [PubMed: 17786044]

Jamieson C, Sharma M, and Henderson BR (2014). Targeting the b-catenin nuclear transport pathway in cancer. Semin. Cancer Biol 27, 20–29. [PubMed: 24820952]

Knockenhauer KE, and Schwartz TU (2016). The nuclear pore complex as a flexible and dynamic gate. Cell 164, 1162–1171. [PubMed: 26967283]

Knudsen KE, and Penning TM (2010). Partners in crime: deregulation of AR activity and androgen synthesis in prostate cancer. Trends Endocrinol. Metab 21, 315–324. [PubMed: 20138542]

Ko¨ hler A, and Hurt E (2010). Gene regulation by nucleoporins and links to cancer. Mol. Cell 38, 6–15. [PubMed: 20385085]

Kralt A, Jagalur NB, van den Boom V, Lokareddy RK, Steen A, Cingolani G, Fornerod M, and Veenhoff LM (2015). Conservation of inner nuclear membrane targeting sequences in mammalian Pom121 and yeast Heh2 membrane proteins. Mol. Biol. Cell 26, 3301–3312. [PubMed: 26179916]

Liang YX, Lu JM, Mo RJ, He HC, Xie J, Jiang FN, Lin ZY, Chen YR, Wu YD, Luo HW, et al. (2016). E2F1 promotes tumor cell invasion and migration through regulating CD147 in prostate cancer. Int. J. Oncol 48, 1650–1658. [PubMed: 26891801]

Liberzon A, Birger C, Thorvaldsdo´ ttir H, Ghandi M, Mesirov JP, and Tamayo P (2015). The Molecular Signatures Database (MSigDB) hallmark gene set collection. Cell Syst. 1, 417–425. [PubMed: 26771021]

Light WH, Brickner DG, Brand VR, and Brickner JH (2010). Interaction of a DNA zip code with the nuclear pore complex promotes H2A.Z incorporation and INO1 transcriptional memory. Mol. Cell 40, 112–125. [PubMed: 20932479]

Mitrousis G, Olia AS, Walker-Kopp N, and Cingolani G (2008). Molecular basis for the recognition of snurportin 1 by importin beta. J. Biol. Chem 283, 7877–7884. [PubMed: 18187419]

Mohr L, Carceles-Cordon M, Woo J, Cordon-Cardo C, Domingo-Domenech J, and Rodriguez-Bravo V (2017). Generation of prostate cancer cell models of resistance to the anti-mitotic agent Docetaxel. J. Vis. Exp (127) 10.3791/56327.

Nakagawa S, Wei L, Song WM, Higashi T, Ghoshal S, Kim RS, Bian CB, Yamada S, Sun X, Venkatesh A, et al.; Precision Liver Cancer Prevention Consortium (2016). Molecular liver cancer prevention in cirrhosis by organ transcriptome analysis and lysophosphatidic acid pathway inhibition. Cancer Cell 30, 879–890. [PubMed: 27960085]

Pascual-Garcia P, and Capelson M (2014). Nuclear pores as versatile platforms for gene regulation. Curr. Opin. Genet. Dev 25, 110–117. [PubMed: 24632227]

Pemberton LF, and Paschal BM (2005). Mechanisms of receptor-mediated nuclear import and nuclear export. Traffic 6, 187–198. [PubMed: 15702987]

Petrylak DP, Tangen CM, Hussain MH, Lara PN, Jr., Jones JA, Taplin ME, Burch PA, Berry D, Moinpour C, Kohli M, et al. (2004). Docetaxel and estramustine compared with mitoxantrone and prednisone for advanced refractory prostate cancer. N. Engl. J. Med 351, 1513–1520. [PubMed: 15470214]

Pollard VW, Michael WM, Nakielny S, Siomi MC, Wang F, and Dreyfuss G (1996). A novel receptor-mediated nuclear protein import pathway. Cell 86, 985–994. [PubMed: 8808633]

Pound CR, Partin AW, Eisenberger MA, Chan DW, Pearson JD, and Walsh PC (1999). Natural history of progression after PSA elevation following radical prostatectomy. JAMA 281, 1591–1597. [PubMed: 10235151]

Raices M, and D'Angelo MA (2012). Nuclear pore complex composition: a new regulator of tissue-specific and developmental functions. Nat. Rev. Mol. Cell Biol 13, 687–699. [PubMed: 23090414]

Rashid F, and Ul Haque A (2011). Frequencies of different nuclear morphological features in prostate adenocarcinoma. Ann. Diagn. Pathol. 15, 414–421. [PubMed: 21849255]

Ren B, Cam H, Takahashi Y, Volkert T, Terragni J, Young RA, and Dynlacht BD (2002). E2F integrates cell cycle progression with DNA repair, replication, and G(2)/M checkpoints. Genes Dev. 16, 245–256. [PubMed: 11799067]

Robinson D, Van Allen EM, Wu YM, Schultz N, Lonigro RJ, Mosquera JM, Montgomery B, Taplin ME, Pritchard CC, Attard G, et al. (2015). Integrative clinical genomics of advanced prostate cancer. Cell 161, 1215–1228. [PubMed: 26000489]

Rodriguez-Bravo V, Maciejowski J, Corona J, Buch HK, Collin P, Kanemaki MT, Shah JV, and Jallepalli PV (2014). Nuclear pores protect genome integrity by assembling a premitotic and Mad1-dependent anaphase inhibitor. Cell 156, 1017–1031. [PubMed: 24581499]

Rodriguez-Bravo V, Carceles-Cordon M, Hoshida Y, Cordon-Cardo C, Galsky MD, and Domingo-Domenech J (2017). The role of GATA2 in lethal prostate cancer aggressiveness. Nat. Rev. Urol 14, 38–48. [PubMed: 27872477]

Rougemaille M, Dieppois G, Kisseleva-Romanova E, Gudipati RK, Lemoine S, Blugeon C, Boulay J, Jensen TH, Stutz F, Devaux F, and Libri D (2008). THO/Sub2p functions to coordinate 3′-end processing with gene-nuclear pore association. Cell 135, 308–321. [PubMed: 18957205]

Ryan CJ, Smith MR, de Bono JS, Molina A, Logothetis CJ, de Souza P, Fizazi K, Mainwaring P, Piulats JM, Ng S, et al.; COU-AA-302 Investigators (2013). Abiraterone in metastatic prostate cancer without previous chemotherapy. N. Engl. J. Med. 368, 138–148. [PubMed: 23228172]

Scher HI, Fizazi K, Saad F, Taplin ME, Sternberg CN, Miller K, de Wit R, Mulders P, Chi KN, Shore ND, et al.; AFFIRM Investigators (2012). Increased survival with enzalutamide in prostate cancer after chemotherapy. N. Engl. J. Med 367, 1187–1197. [PubMed: 22894553]

Schuhmacher M, Kohlhuber F, Ho¨ lzel M, Kaiser C, Burtscher H, Jarsch M, Bornkamm GW, Laux G, Polack A, Weidle UH, and Eick D (2001). The transcriptional program of a human B cell line in response to Myc. Nucleic Acids Res. 29, 397–406. [PubMed: 11139609]

Seidenfeld J, Samson DJ, Hasselblad V, Aronson N, Albertsen PC, Bennett CL, and Wilt TJ (2000). Single-therapy androgen suppression in men with advanced prostate cancer: a systematic review and meta-analysis. Ann. Intern. Med 132, 566–577. [PubMed: 10744594]

Simon DN, and Rout MP (2014). Cancer and the nuclear pore complex. Adv. Exp. Med. Biol 773, 285–307. [PubMed: 24563353]

Soderholm JF, Bird SL, Kalab P, Sampathkumar Y, Hasegawa K, Uehara-Bingen M, Weis K, and Heald R (2011). Importazole, a small molecule inhibitor of the transport receptor importin-b. ACS Chem. Biol 6, 700–708. [PubMed: 21469738]

Stavru F, Nautrup-Pedersen G, Cordes VC, and Go¨ rlich D (2006). Nuclear pore complex assembly and maintenance in POM121- and gp210deficient cells. J. Cell Biol 173, 477–483. [PubMed: 16702234]

Sweeney CJ, Chen YH, Carducci M, Liu G, Jarrard DF, Eisenberger M, Wong YN, Hahn N, Kohli M, Cooney MM, et al. (2015). Chemohormonal therapy in metastatic hormone-sensitive prostate cancer. N. Engl. J. Med 373, 737–746. [PubMed: 26244877]

Taddei A, Van Houwe G, Hediger F, Kalck V, Cubizolles F, Schober H, and Gasser SM (2006). Nuclear pore association confers optimal expression levels for an inducible yeast gene. Nature 441, 774–778. [PubMed: 16760983]

Talamas JA, and Hetzer MW (2011). POM121 and Sun1 play a role in early steps of interphase NPC assembly. J. Cell Biol 194, 27–37. [PubMed: 21727197]

Tannock IF, de Wit R, Berry WR, Horti J, Pluzanska A, Chi KN, Oudard S, The´ odore C, James ND, Turesson I, et al.; TAX 327 Investigators (2004). Docetaxel plus prednisone or mitoxantrone plus prednisone for advanced prostate cancer. N. Engl. J. Med 351, 1502–1512. [PubMed: 15470213]

Thompson TC, Southgate J, Kitchener G, and Land H (1989). Multistage carcinogenesis induced by ras and myc oncogenes in a reconstituted organ. Cell 56, 917–930. [PubMed: 2538247]

Torre LA, Bray F, Siegel RL, Ferlay J, Lortet-Tieulent J, and Jemal A (2015). Global cancer statistics, 2012. CA Cancer J. Clin 65, 87–108. [PubMed: 25651787]

Van de Vosse DW, Wan Y, Lapetina DL, Chen WM, Chiang JH, Aitchison JD, and Wozniak RW (2013). A role for the nucleoporin Nup170p in chromatin structure and gene silencing. Cell 152, 969–983. [PubMed: 23452847]

Vidal SJ, Rodriguez-Bravo V, Quinn SA, Rodriguez-Barrueco R, Lujambio A, Williams E, Sun X, de la Iglesia-Vicente J, Lee A, Readhead B, et al. (2015). A targetable GATA2-IGF2 axis confers aggressiveness in lethal prostate cancer. Cancer Cell 27, 223–239. [PubMed: 25670080]

Wang CI, Chien KY, Wang CL, Liu HP, Cheng CC, Chang YS, Yu JS, and Yu CJ (2012). Quantitative proteomics reveals regulation of karyopherin subunit alpha-2 (KPNA2) and its potential novel cargo proteins in nonsmall cell lung cancer. Mol. Cell. Proteomics 11, 1105–1122. [PubMed: 22843992]

Wente SR, and Rout MP (2010). The nuclear pore complex and nuclear transport. Cold Spring Harb. Perspect. Biol 2, a000562. [PubMed: 20630994]

Williams ES, Rodriguez-Bravo V, Chippada-Venkata U, De Ia Iglesia-Vicente J, Gong Y, Galsky M, Oh W, Cordon-Cardo C, and Domingo-Domenech J (2015). Generation of prostate cancer patient derived xenograft models from circulating tumor cells. J. Vis. Exp (105), 53182. [PubMed: 26555435]

Yavuz S, Santarella-Mellwig R, Koch B, Jaedicke A, Mattaj IW, and Antonin W (2010). NLS-mediated NPC functions of the nucleoporin Pom121. FEBS Lett. 584, 3292–3298. [PubMed: 20624389]

Yu D, and Thomas-Tikhonenko A (2002). A non-transgenic mouse model for B-cell lymphoma: in vivo infection of p53-null bone marrow progenitors by a Myc retrovirus is sufficient for tumorigenesis. Oncogene 21, 1922–1927. [PubMed: 11896625]

Zheng C, Ren Z, Wang H, Zhang W, Kalvakolanu DV, Tian Z, and Xiao W (2009). E2F1 Induces tumor cell survival via nuclear factor-kappaB-dependent induction of EGR1 transcription in prostate cancer cells. Cancer Res. 69, 2324–2331. [PubMed: 19276347]

Zong Y, and Goldstein AS (2013). Adaptation or selection–mechanisms of castration-resistant prostate cancer. Nat. Rev. Urol 10, 90–98. [PubMed: 23247694]

Highlights

- Nuclear pores display a distinct Nup composition during progression to lethal PC
- Nup POM121 impacts on PC aggressiveness by enhancing bnimportin β function
- POM121 promotes nuclear import of key transcription factors driving PC
- Targeting the POM121-importin β axis decreases the aggressiveness of PC tumors

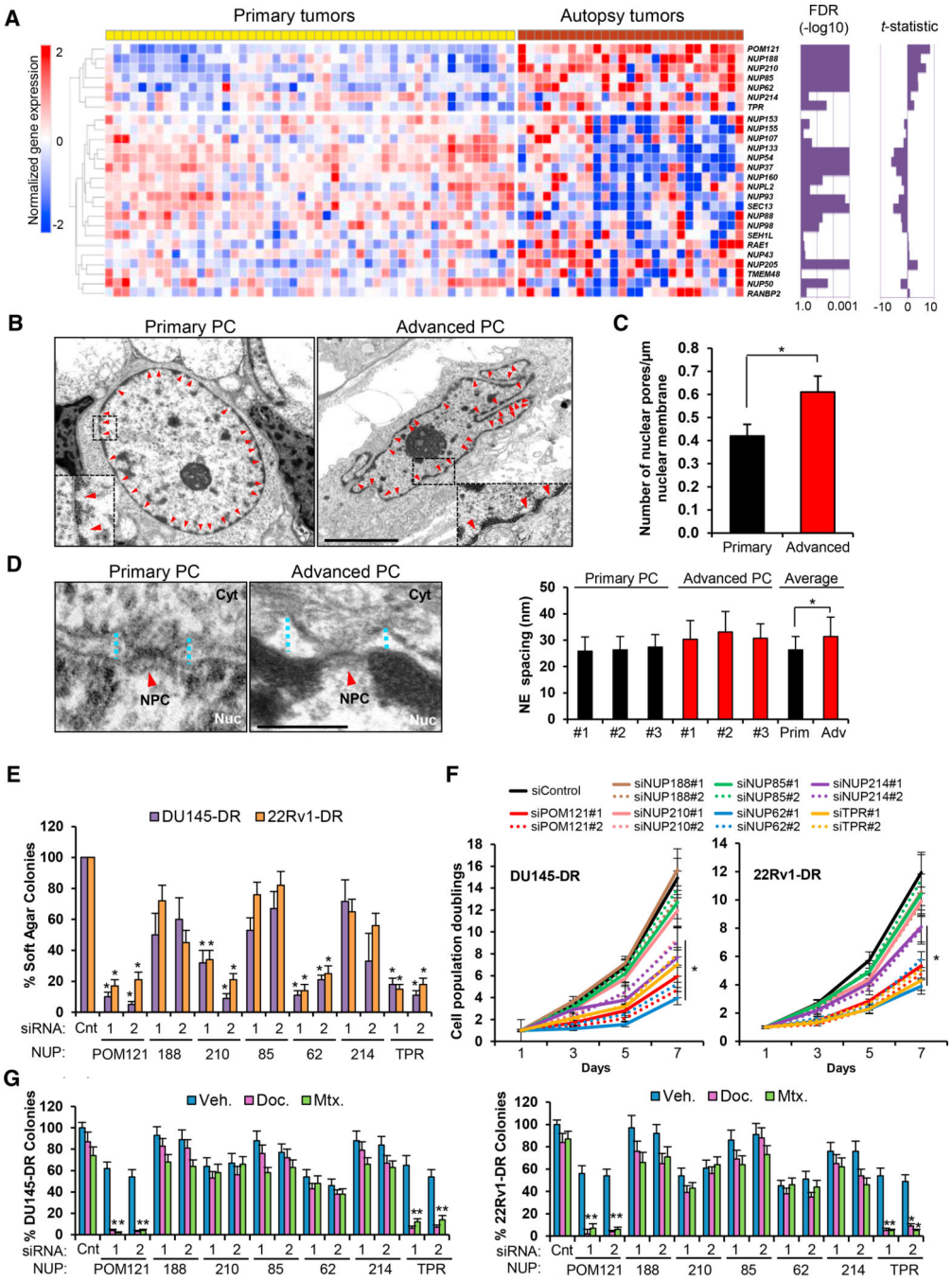

Figure 1. Advanced Lethal PC NPCs Display a Distinct Nup Composition that Contributes to PC Aggressiveness

(A) Heatmap of Nups in primary and metastatic warm-autopsy PC tumor tissues (GSE35988). Magnitude (t-statistic) and statistical significance (false discovery rate [FDR]) of differential expression between the groups are shown as bar graph for each Nup gene. Red and blue colors indicate high and low gene expression, respectively.

(B–D) Representative transmission electron microscopy imaging (scale bar, 5 µm) (B) and quantification of (C) number of pores and (D) NE spacing in primary (n = 3) and advanced

(n = 3) PC cells from human tumor samples. Red arrows point to NPCs. Blue dot lines point to NE spacing. Scale bar, 500 nm.

(E) Quantification of soft agar colony formation assays of aggressive PC cells transfected with control siRNA or two siRNAs targeting each upregulated Nup.

(F) Quantification of cell population doublings from (E).

(G) Quantification of colony formation assays of cells from (E) following 72 hr treatment with docetaxel (125 nM) and mitoxantrone (500 nM). Data represent the mean ± SD of 3 experiments. *p ≤0.05. See also Figure S1 and Table S1.

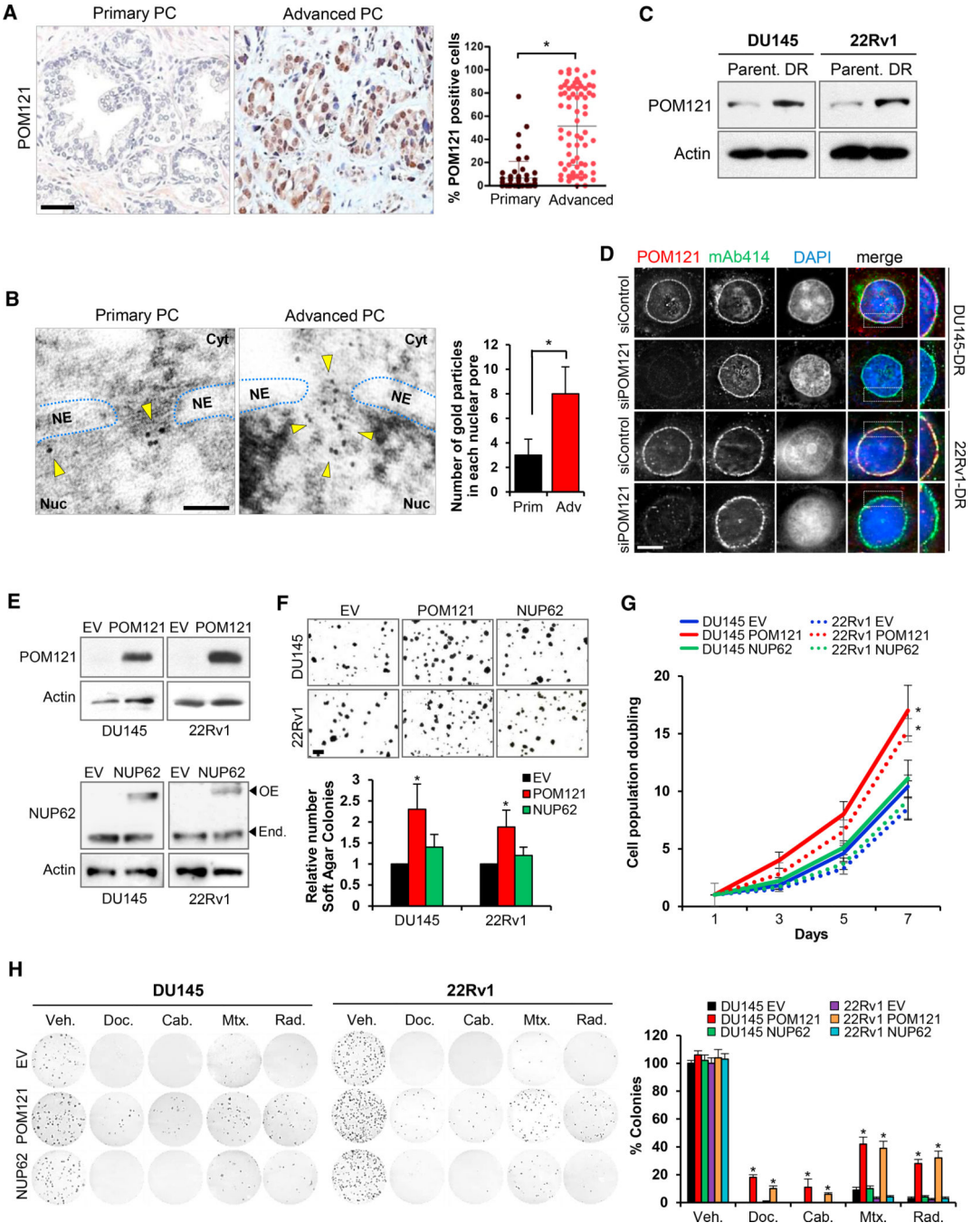

Figure 2. Nucleoporin POM121 Promotes Tumorigenesis, Proliferation, and Survival to Standard Therapies in PC Cells

(A) Immunohistochemistry and quantification of POM121-positive cells during disease progression in a series (n = 124) of human paraffin-embedded PC tissues.Scale bar, 100 μm. (B) Transmission electron microscopy images and quantification of POM121 Immunogold stained protein localized in NPCs of PC cells from primary (n = 3) and advanced (n = 3) PC tissues. 120 NPCs where analyzed for each tumor sample from a minimum of 5 images. Scale bar, 100 nm.

(C) Immunoblot of POM121 in aggressive PC cells (DU145-DR and 22Rv1-DR) compared to parental cells (DU145 and 22Rv1).
(D) Immunofluorescence of POM121 and Nups (NUP214, NUP98, and NUP62) detected by mAb414 antibody in aggressive PC cells transfected with control andPOM121 siRNAs. Scale bar, 5 μm.
(E) Immunoblot of POM121 and NUP62 in parental cells transfected with an empty, POM121, or NUP62 vector.
(F) Soft agar colony formation assays and quantifications of cells from (E). Scale bar, 100 mm.
(G) Quantification of cell population doublings of cells from (E).
(H) Colony formation assays and quantification of cells from (E) following 72 hr treatment with docetaxel (5 nM), cabazitaxel (1 nM), mitoxantrone (5 nM), and singledose radiation (2 Gys). Data represent the mean ± SD of 3 experiments. *$p < 0.05$. See also Figure S2

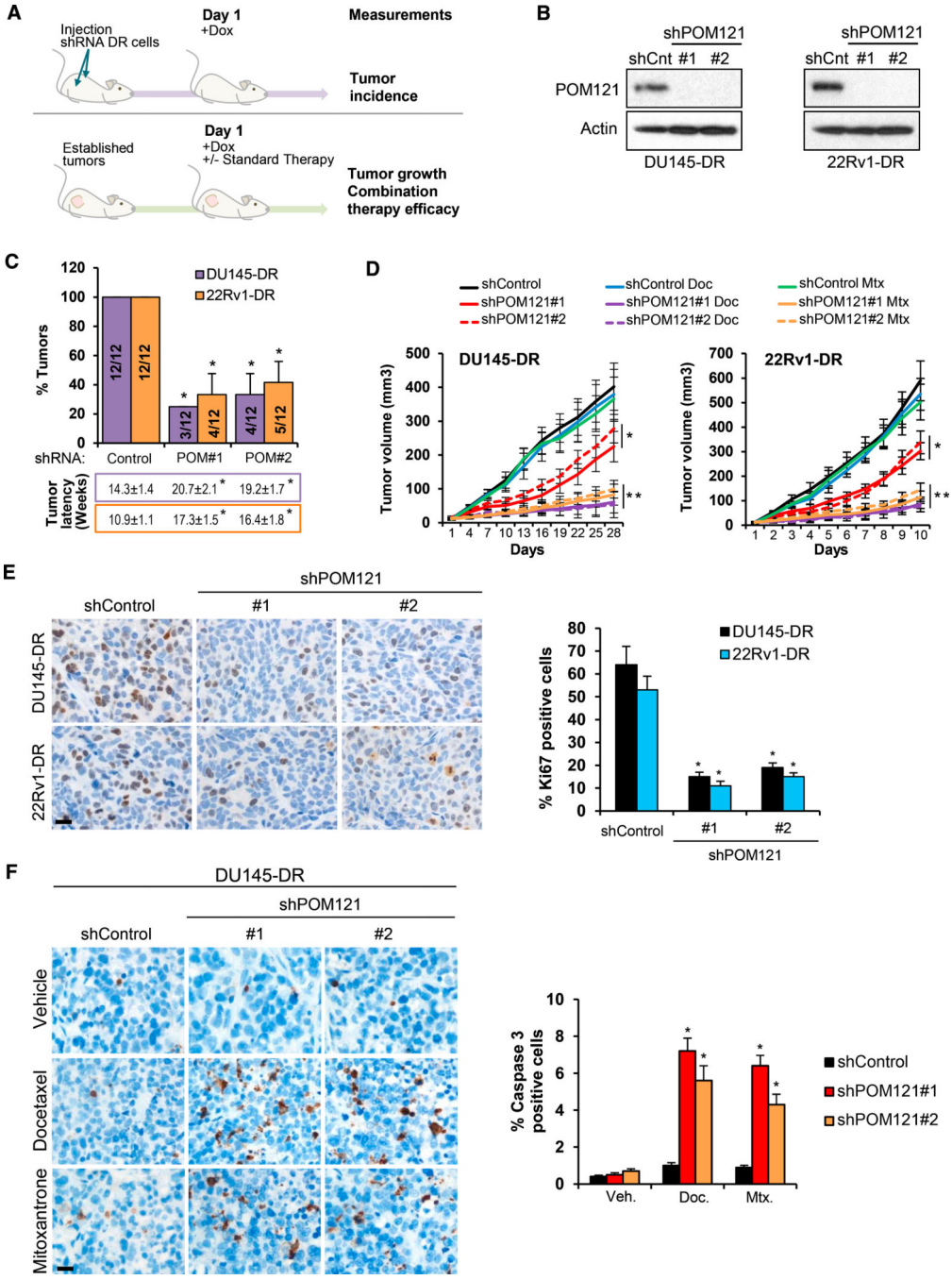

Figure 3. In Vivo POM121 Depletion Decreases PC Aggressiveness

(A) Experimental design used to test the *in vivo* effects of targeting POM121 on tumorigenesis, tumor growth, and response to therapy.

(B) Immunoblot of POM121 in DU145-DR and 22RV1-DR cells transduced with a control shRNA and two inducible shRNAs targeting POM121 after 72 hr ofdoxycycline (1 μg/mL) exposure.

(C) Tumor incidence and latency of 100 cells from (B) subcutaneously injected into NSG mice. 12 injection sites for each experimental condition were monitored weekly during 6 months for tumor formation.

(D) Volumes of DU145-DR and 22Rv1-DR control or POM121 doxycycline-induced shRNAs subcutaneous xenografts after 28 days of combination treatmentwith vehicle, docetaxel (10 mg/kg intraperitoneally [i.p.] weekly), or mitoxantrone (10 mg/kg i.p. weekly). Tumor volumes of 12 xenografts for each treatment condition where analyzed. *p ≤0.05 = Comparison between control and shPOM121. **p ≤ 0.05 = comparison between shControl and shPOM121 treated with docetaxel or mitoxantrone.

(E) Immunohistochemistry and quantification of Ki67 expression in tumor xenografts from (C). Scale bar, 100 μm.

(F) Immunohistochemistry and quantification of cleaved caspase 3 expression in DU145-DR tumor xenografts from (D). Scale bar, 100 μm. Data represent the mean ± SD. *p < 0.05. See also Figure S3

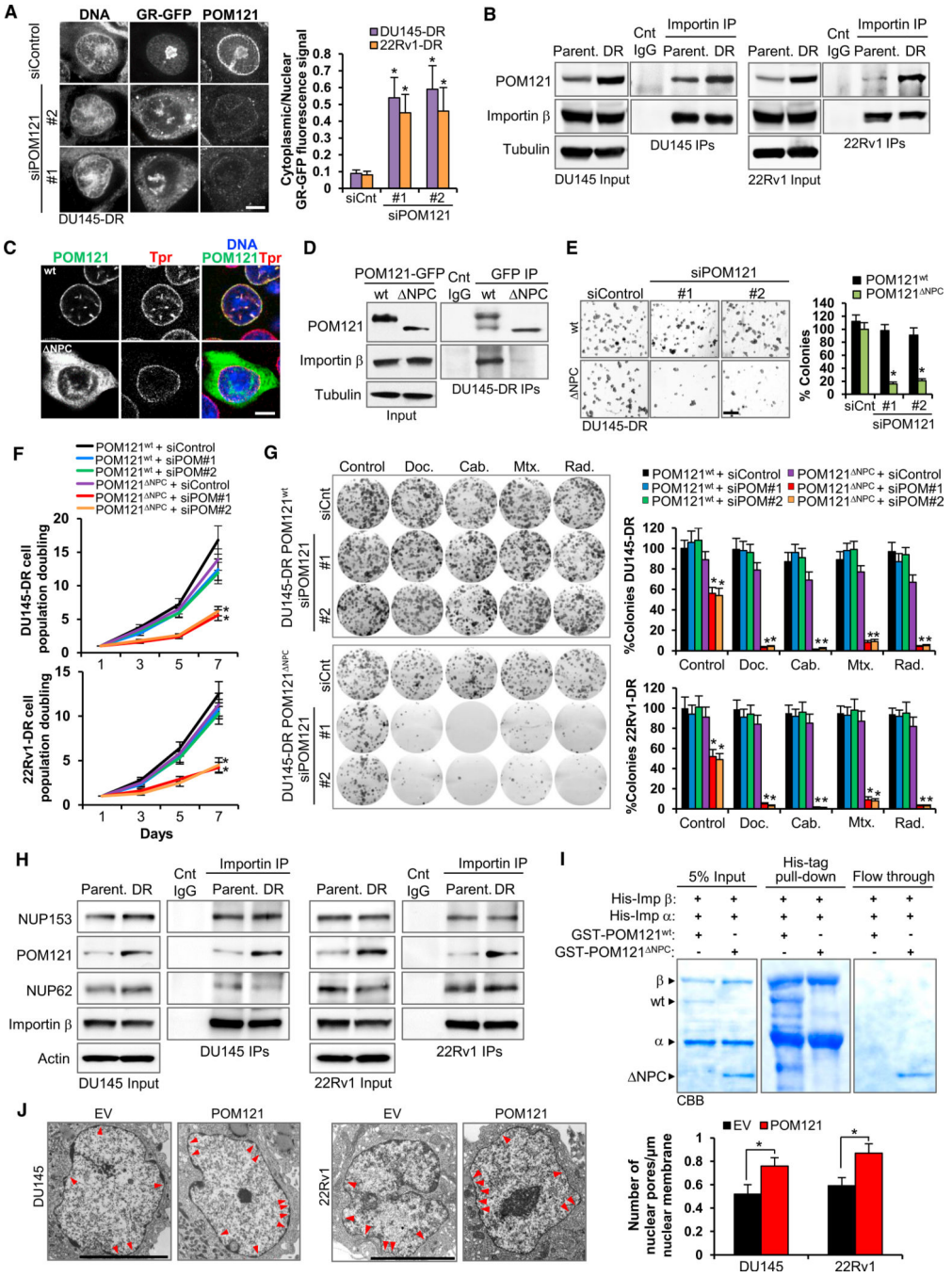

Figure 4. POM121 Regulates PC Cell Aggressiveness through Its Interaction with the Nuclear Import Machinery

(A) GFP and POM121 immunofluorescence and quantification of cytoplasmic versus nuclear fluorescent signal in DU145-DR and 22Rv1-DR cells stablyexpressing a (GR)-GFP reporter after transfecting control siRNA and two siRNAs targeting POM121, treated with dexamethasone (100 nM) and the export XPO-1 inhibitor selinexor (1 μM) for 10 min. Data represent the mean ± SD quantification of 50 cells for each condition. Scale bar, 5 μm.

(B) Immunoblots of POM121 after immunoprecipitation of importin β in parental and aggressive PC cells.

(C) GFP immunofluorescence confocal images of WT POM121-GFP-siRNA-resistant and ΔNPC POM121-GFP-siRNA-resistant DU145-DR cells. NE localization and integrity is determined by TPR staining. Scale bar, 5 μm.
(D) POM121 immunoblot after anti-GFP immunoprecipitation in cells from (C).
(E) Soft agar colony formation assays and quantification of cells from (C) transfected with control siRNA or two siRNAs targeting POM121. Scale bar, 100 μm.
(F) Quantification of cell population doublings of cells from (E).
(G) Colony formation assays and quantifications of cells from (E) following 72 hr treatment with docetaxel (125 nM), cabazitaxel (25 nM), mitoxantrone (500 nM),and single dose radiation (5 Gys).
(H) Immunoblots of FG-Nups (NUP153, POM121, and NUP62) following immunoprecipitation of importin β in paired parental and aggressive PC cells. (I) SDS-PAGE Coomassie brilliant blue (CBB) of GST-tagged human WT or ΔNPC POM121 tested for binding to recombinant human His-tagged importins α and β after His-tag in vitro pull-down assays.
(J) Transmission electron microscopy images and quantification of number of NPCs in parental cells transduced with an empty or POM121 vector. Red arrows point to NPCs. Scale bar, 5 μm. Data represent the mean ± SD. *$p < 0.05$. See also Figure S4

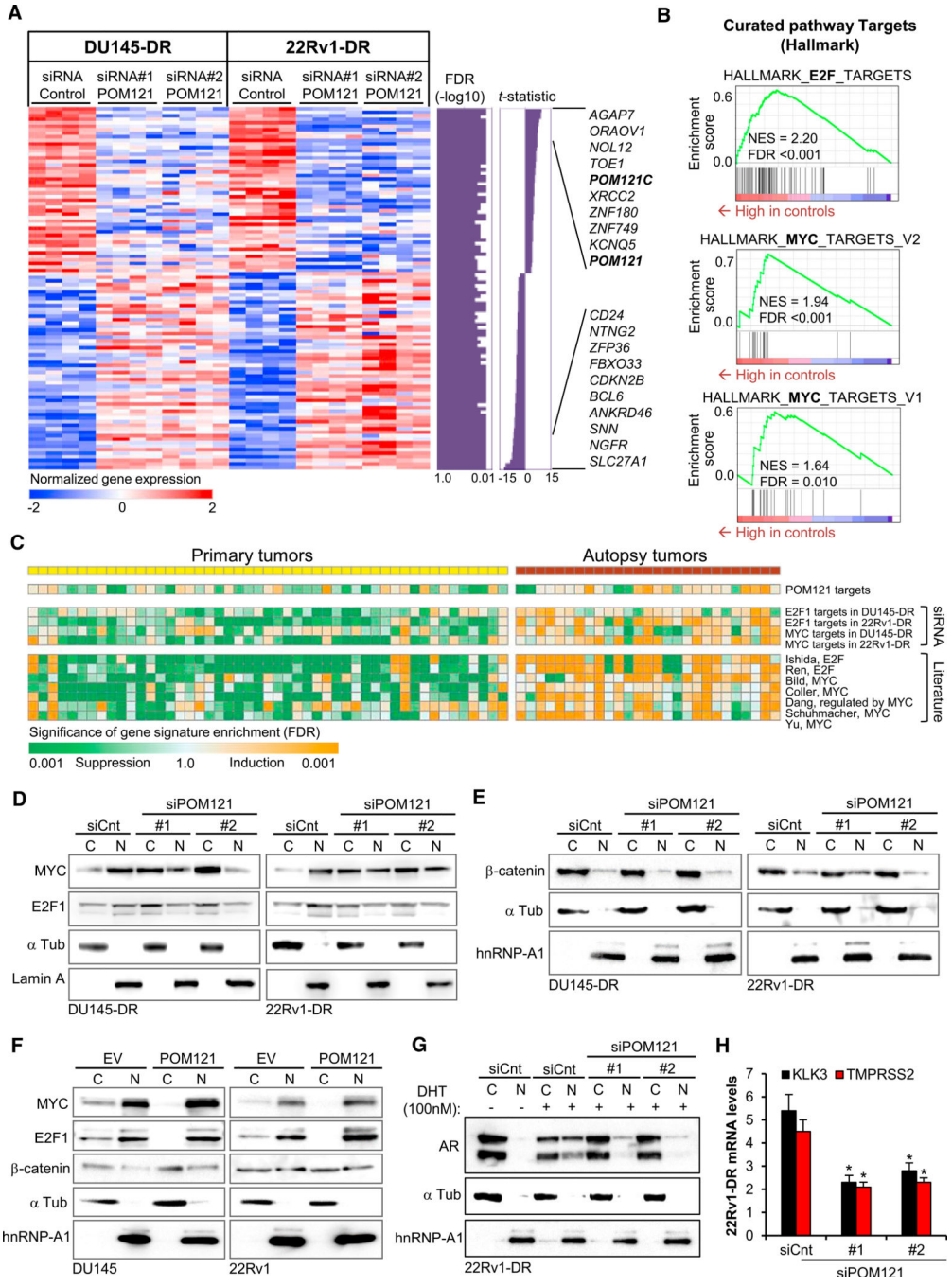

Figure 5.

POM121 Facilitates the Selective Nuclear Import of Cell Tumorigenic-, Proliferation-, and Survival-Conferring Transcription Factors in Lethal PC

(A) Expression pattern of genes modulated by siRNA-mediated POM121 knockdown in DU145-DR and 22Rv1-DR cells. Magnitude (t-statistic) and statistical significance (false discovery rate [FDR]) of differential expression between the groups are shown as bar graph for each gene. Red and blue colors indicate high and low gene expression, respectively.

(B) Modulation of E2F1 and MYC target gene signatures determined by transcriptome meta-analysis by siRNA-mediated POM121 knockdown in PC cells (GeneSet Enrichment Analysis [GSEA]).

(C)Modulation of POM121, MYC and E2F1 target gene signatures determined by siRNA-mediated in vitro gene knockdown or reported in literature (Table S3) in primary and warm-autopsy tumor tissues (GSE35988). Orange and green colors indicate statistical significance (FDR) of induction and suppression of the target gene signatures, respectively (modified GSEA).

(D)Immunoblot of MYC and E2F1 levels in the nucleoplasm and cytoplasm of aggressive PC cells after 72 hr of being transfected with control siRNA and twosiRNAs targeting POM121.

(E) Immunoblot of β-catenin and hnRNP-A1 levels in the nucleoplasm and cytoplasm of cells from (D).

(F) Immunoblots of MYC, E2F1, and β-catenin levels in the nucleoplasm and cytoplasm of parental cells transduced with an empty vector (EV) or POM121 vector.

(G) Immunoblot of AR levels in the nucleoplasm and cytoplasm of 22Rv1-DR cells transfected with control siRNA and two siRNAs targeting POM121 (72 hr) and further cultured in FBS free conditions and exposed to 100 nM dihydrotestosterone (DHT) during 18 hr.

(H) Quantitative analysis of AR target genes KLK3 and TMPRSS2 mRNA levels of cells from (G). Data represent the mean ± SD of 3 experiments. *$p < 0.05$. See also Figure S5 and Tables S2–S5.

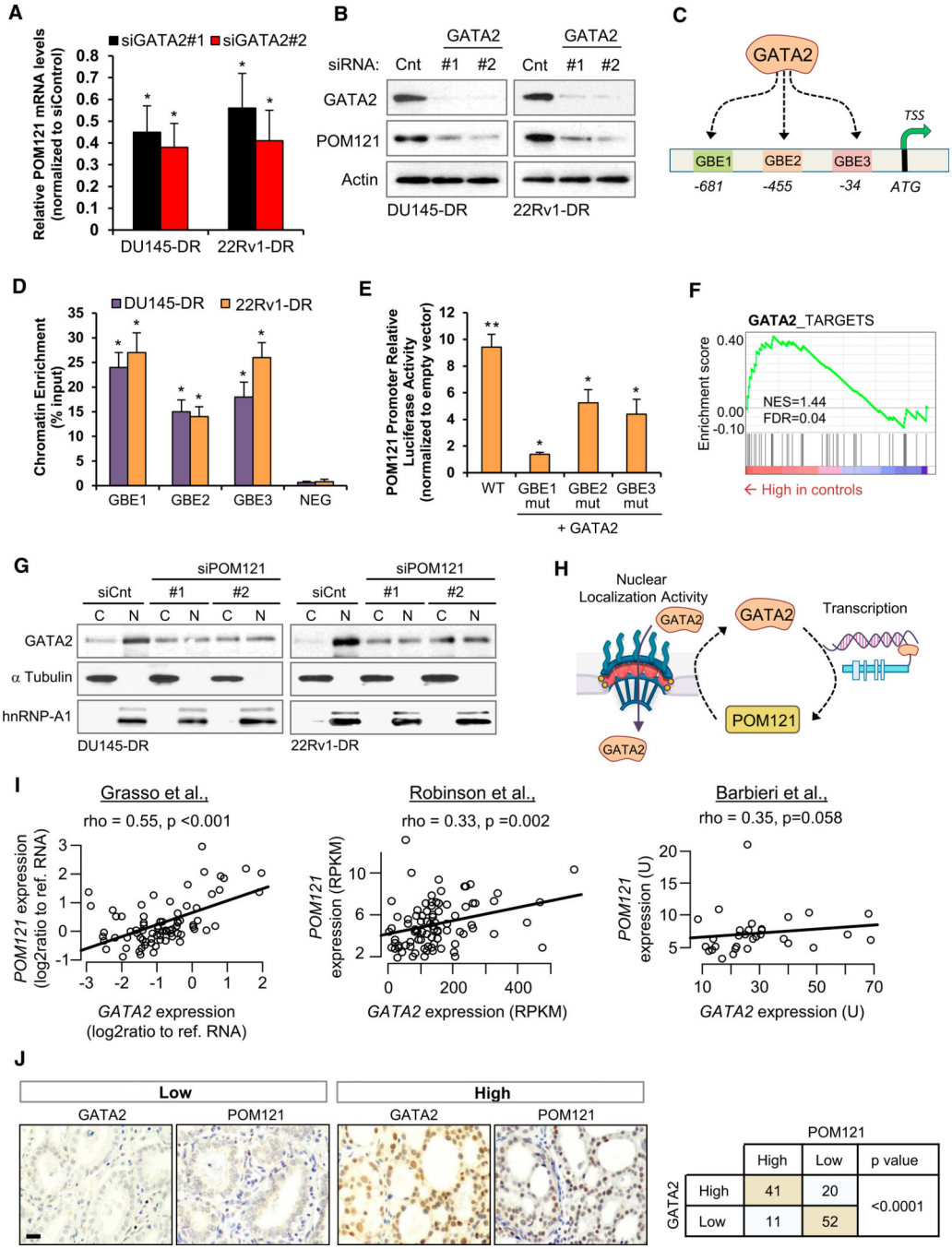

Figure 6. A GATA2-POM121 Regulatory Feedback Loop Modulates PC Aggressiveness

(A and B) mRNA (A) and protein (B) levels of POM121 in aggressive PC cells transfected with siRNA control and two siRNAs targeting GATA2.

(C) Representation of three predicted GATA2 binding elements (GBEs) in the POM121 promoter region.

(D) ChIP-qPCR of GATA2 occupancy at GBE1, GBE2, GBE3, and flanking control region (NEG) in the POM121 promoter of aggressive PC cells.

(E) Luminescence analysis of HEK293 cells following co-transfection with an empty or GATA2 expression vector, a POM121 promoter luciferase reporter (wildtype [WT], mutated GBE1 [mutGBE1], mutated GBE2 [mutGBE2], or mutated GBE3 [mutGBE3]), and a Renilla transfection control. *$p < 0.05$. **$p < 0.01$ relative to control vector.
(F) Modulation of POM121 target gene signature in GATA2-depleted cells (accession number GSE58966). GSEA. NES, normalized enrichment score; FDR, falsediscovery rate.
(G) Immunoblot of GATA2 levels in the nucleoplasm and cytoplasm of aggressive PC cells after 72 hr of being transfected with control siRNA and two siRNAstargeting POM121.
(H) Representation of the GATA2-POM121-positive feedback regulation. GATA2 regulates the transcription of POM121 and POM121 regulates the nuclear localization of GATA2.
(I) Correlation between POM121 and GATA2 gene expression levels in public available clinical PC databases (accession numbers GSE35988, dbGap: phs000915.v1.p1 and dbGaP: phs000447.v1.p1). Spearman correlation test rho and p value are shown.
(J) Immunohistochemical expression of POM121 and GATA2 in a PC tissue samples. Statistically association between proteins was analyzed by χ^2 test. Data represent the mean ± SD of 3 experiments. Scale bar, 100 μm. *$p < 0.05$. See also Figure S6.

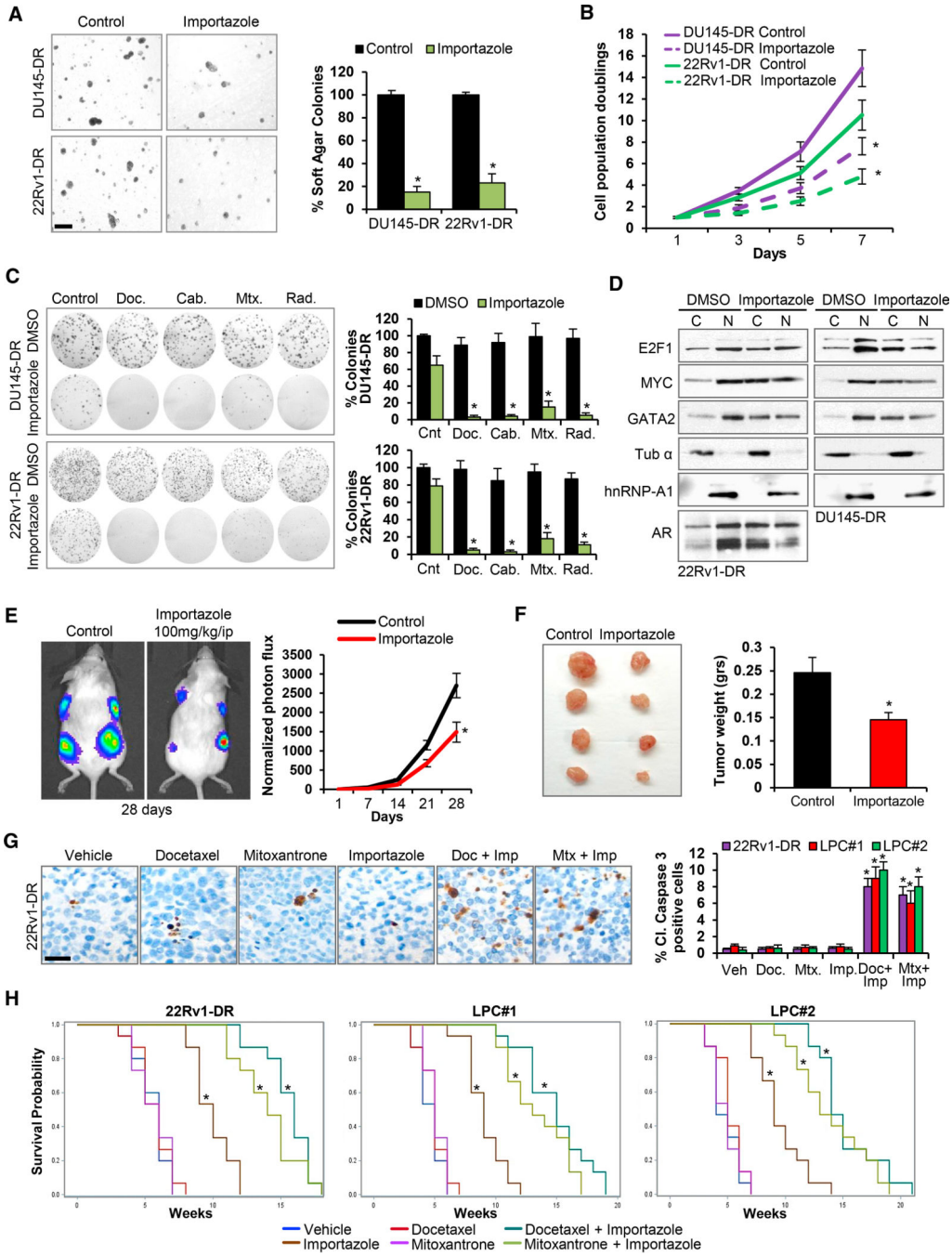

Figure 7. Targeting the POM121-Importin β Axis Decreases the Growth and Survival of Lethal PC Pre-clinical Models

(A) Soft agar colony formation assays and quantification of aggressive PC cells treated during 72 hr with vehicle (Control) or Importazole 1 μM. Scale bar, 100 μm.

(B) Quantification of cell population doublings of cells from (A).

(C) Representative colony formation assays and quantification of cells from (A) following 72 hr treatment with docetaxel (125 nM), cabazitaxel (25 nM), mitoxantrone (500 nM), and single dose radiation (5 Gys).

(D) Immunoblot of MYC, E2F1, GATA2, and AR levels in the nucleoplasm and cytoplasm of aggressive PC cells after 72 hr treatment with DMSO orImportazole 1 μM.
(E) Bioluminescence analysis of mice bearing 22Rv1-DR luciferase-expressing xenografts treated with vehicle or Importazole (100 mg/kg i.p. daily 5 days a week) during 28 days. Data represent the mean ± SD of 15 mice for each treatment condition.
(F) Representative image and weight quantification of tumor xenografts from (E). Data represent the mean ± SD of 15 mice for each treatment group. (G) Representative immunohistochemistry images and quantification of cleaved caspase 3 expression in 22Rv1-DR, LPC#1, and LPC#2 xenografts after 7 days of treating mice with docetaxel (10 mg/kg i.p. weekly) and mitoxantrone (10 mg/kg i.p. weekly) alone or in combination with Importazole (100 mg/kg i.p. daily).Scale bar, 50 μm.
(H) Kaplan-Meier survival curves of NSG mice following intracardially injection of 22Rv1-DR, LPC#1, and LPC#2 cells treated as in (G). 15 mice for each treatment group were analyzed. Data represent the mean ± SD of 3 experiments. *$p < 0.05$. See also Figure S7.

REAGENT or RESOURCE	SOURCE	IDENTIFIER
Antibodies		
Rabbit polyclonal anti-POM121	GeneTex	GTX102128; RRID: AB_10732546
Rabbit polyclonal anti-NUP62	GeneTex	GTX107973; RRID: AB_1951041
Rabbit polyclonal anti-GATA2	Sigma-Aldrich	HPA005633; RRID: AB_1078954
Mouse monoclonal anti- hnRNP-A1	Sigma-Aldrich	R-4528; RRID: AB_261962
Mouse monoclonal anti-ß-Actin	Sigma-Aldrich	A-5441; RRID: AB_476744
Mouse monoclonal anti-Mab414	Abcam	ab24609; RRID: AB_448181
Rabbit polyclonal anti-TPR	Abcam	ab84516; RRID: AB_1861454
Rabbit polyclonal anti-NUP153	Abcam	ab84872; RRID: AB_1859766
Rabbit polyclonal anti-Lamin A	Abcam	ab26300; RRID: AB_775965
Rabbit monoclonal anti-c MYC	Abcam	ab32072; RRID: AB_731658
Rabbit monoclonal anti-E2F1	Abcam	ab179445
Mouse monoclonal anti-fluorescent protein (GFP)	Santa Cruz Biotechnology	SC-9996; RRID: AB_627695
Rabbit polyclonal anti-karyopherin ß1 (H-300)	Santa Cruz Biotechnology	SC-11367; RRID: AB_2265549
Mouse monoclonal anti-karyopherin a2 (B-9)	Santa Cruz Biotechnology	SC-55538; RRID: AB_831493
Rabbit polyclonal anti-androgen receptor (N-20)	Santa Cruz Biotechnology	SC-816; RRID: AB_1563391
Mouse monoclonal anti-Tubulin a (DM1A)	Millipore	CP06; RRID: AB_2617116
Rabbit polyclonal anti-cleaved caspase-3	Cell Signaling	9661S; RRID: AB_2341188
Mouse monoclonal anti-ß-catenin	Invitrogen	13–8400; RRID: AB_2533039
Anti-mouse IgG, Horseradish Peroxidase	GE	NA931; RRID: AB_772210
Anti-Rabbit IgG, Horseradish Peroxidase	GE	NA934; RRID: AB_2722659
Alexa Fluor 488 AffiniPure Donkey anti-Mouse IgG (H+L)	Jackson ImmunoResearch	715–545-150; RRID: AB_2340846
Rhodamine (TRITC) AffiniPure Donkey anti-Rabbit IgG (H +L)	Jackson ImmunoResearch	711–025-152; RRID: AB_2340588
Rabbit polyclonal GATA2 (H-116)	Santa Cruz	sc-9008; RRID: AB_2294456
Rabbit polyclonal IgG Control (Chip grade)	Abcam	ab171870; RRID: AB_2687657
Goat anti rabbit IgG with 10 nm AuNP	Electron Microscopy Sciences	25108
Bacterial and Virus Strains		
NEB 5-alpha competent E. coli	New England BioLabs	2987H
Biological Samples		
Prostate cancer paraffin embedded tumor samples	Thomas Jefferson University GU Biorepository	See STAR Methods
Prostate cancer paraffin embedded tumor samples	Mount Sinai GU Biorepository	See STAR Methods
Chemicals, Peptides, and Recombinant Proteins		
Docetaxel	Selleck Chemicals	S1148
Cabazitaxel	Selleck Chemicals	S3022
Mitoxantrone	Selleck Chemicals	S2485
Importazole	Selleck Chemicals	S8446
Selinexor	Selleck Chemicals	S7252

REAGENT or RESOURCE	SOURCE	IDENTIFIER
Matrigel	Corning	354230
Crystal violet	Acros Organics	229641000
Difco Noble Agar	BD Biosciences	214230
Dynabeads Protein G	Invitrogen	10004D
Dynabeads Protein A	Invitrogen	10002D
XeneLight D-Luciferin Potassium Salt	PerkinElmer	122799
Critical Commercial Assays		
RNeasy Mini kit	QIAGEN	74106
SuperScript III First-Strand Synthesis SuperMix Kit	Thermo Scientific	18080400
NE-PER Nuclear and Cytoplasm Extraction Reagents	Thermo Scientific	78833
Dual-Luciferase-Assay System	Promega	E1910
TruSeq ChIP Library Preparation Kit	Illumina	IP-202–1012
Deposited Data		
RNA-seq raw data of POM121-knockdown	This paper	GEO: GSE103637
RNA-seq raw data of GATA2-knockdown	Vidal etal., 2015	GEO: GSE58966
Transcriptome of prostate cancer patient samples	Grasso et al., 2012	GEO: GSE35988
Transcriptome of prostate cancer patient samples	Robinson et al., 2015	dbGap: phs000915.v1.p1.
Transcriptome of prostate cancer patient samples	Barbieri et al., 2012	dbGaP: phs000447.v1.p1
Experimental Models: Cell Lines		
DU145	ATCC	ATCC HTB-81
22Rv1	ATCC	ATCC CRL-2505
LNCaP	ATCC	ATCC CRL-1740
HEK293	ATCC	ATCC CRL-1573
DU145-DR	Domingo-Domenech et al., 2012; Mohr et al., 2017	N/A
22Rv1 -DR	Domingo-Domenech et al., 2012; Mohr et al., 2017	N/A
LPC#1	Vidal et al., 2015; Williams et al., 2015	N/A
LPC#2	Vidal et al., 2015; Williams et al., 2015	N/A
Experimental Models: Organisms/Strains		
NOD.Cg-Prkdc^{scid} IL2rg^{tm1Wjl} (NSG) mice	Jackson mice	005557
Oligonucleotides		
siRNA Control#1	Ambion	AM4636
siRNA POM121 #1	Life Technologies	s59623
siRNA POM121#2	Life Technologies	s19145
siRNA NUP188#1	Life Technologies	s23964
siRNA NUP188#2	Life Technologies	s23966
siRNA NUP210#1	Life Technologies	s23331
siRNA NUP210#2	Life Technologies	s23332

REAGENT or RESOURCE	SOURCE	IDENTIFIER
siRNA NUP85#1	Life Technologies	s36610
siRNA NUP85#2	Life Technologies	s36611
siRNA NUP62#1	Life Technologies	s24247
siRNA NUP62#2	Life Technologies	s24248
siRNA NUP214#1	Life Technologies	s15547
siRNA NUP214#2	Life Technologies	s15549
siRNA TPR#1	Life Technologies	s14353
siRNA TPR#2	Life Technologies	s14354
shRNA POM121.486	This paper	N/A
shRNA POM121.834	This paper	N/A
shRNA non-targeting Renilla control	This paper	N/A
Primers for POM121 RT-PCR	This paper	N/A
Forward ACATTCCCTTTGGCTCAA		
Reverse CAGCCGGGGCTGCAGAGT		
Primers for NUP188 RT-PCR	This paper	N/A
Forward ACATTGGCGGCGATTGTTAGA		
Reverse GCTGATTCTTAAACCCAGTTCCT		
Primers for NUP210 RT-PCR	This paper	N/A
Forward TGGTCTTCGAGTGGACGATTG		
Reverse GCAGGGCGTACATTCTTGTAG		
Primers for NUP85 RT-PCR	This paper	N/A
Forward GGCGAGCCAACAGTCACTTT		
Reverse ACTCTTCGTCAATTCTCTGGAGG		
Primers for NUP62 RT-PCR	This paper	N/A
Forward GGAACAGCGACTCTTGCTTC		
Reverse GGTGCTCGATATGGCATTAGTG		
Primers for NUP214 RT-PCR	This paper	N/A
Forward TGACTCCCCTGAGGAATTGC		
Reverse GCGAAGACCAGACCATATTTGTT		
Primers for TPR RT-PCR	This paper	N/A
Forward AACGCCAGCGTGAGGAATATG		
Reverse ATTACGTGGTTACCCCTTGCT		
Primers for POM121 GBE1 mutant cloning	This paper	N/A
Forward CAGCTTTATTAAggggTAATTCACATACCATGC Reverse GCATGGTATGTGAATTAccccTTAATAAAGCTG		
Primers for POM121 GBE2 mutant cloning	This paper	N/A
Forward CAAAATCCACCCggggTCTGGGCCATG Reverse CATGGCCCAGAccccGGGTGGATTTTG		
Primers for POM121 GBE3 mutant cloning	This paper	N/A
Forward GTGCACGCTGGggggTTTAAGTCTCC		

REAGENT or RESOURCE	SOURCE	IDENTIFIER
Reverse GGAGACTTAAAccccCCAGCGTGCAC		
Primers for POM121 GBE1 ChIP q-PCR	This paper	N/A
Forward TGAATGGCTGAGGAAACTGA		
Reverse TAGGGCTAGGGAGTGGGTTT		
Primers for POM121 GBE2 ChIP q-PCR	This paper	N/A
Forward CCTAGCCCTAGGCAACCACT		
Reverse CTCCAGCACAGCCTGTTACC		
Primers for POM121 GBE3 ChIP q-PCR	This paper	N/A
Forward TTCCAAACCAGTTGGGTCTC		
Reverse GTCCCTGACACTCGCTATGG		
Primers for Negative control ChIP q-PCR	This paper	N/A
Forward TGCATCCATATTTTGCAGGA		
Reverse GAATGATTGGCCCGTAGAGA		
Recombinant DNA		
rtTA3-IRES-EcoR-Puro (RIEP2)	gift from Dr. Scott Lowe	N/A
TRIN-E vector	gift from Dr. Scott Lowe	N/A
pET30a GST-POM121 WT (266–700)	This paper (Genescript)	N/A
pET30a GST-POM121 ANPC (510–700)	This paper (Genescript)	N/A
Human 6 × His-Importin ß1	Novoprotein	CP58
Human 6 × His-Importin a2	Novoprotein	CE62
pET28-MBP POM121 NLS (291–320) wild type (wt)	Kralt et al., 2015	N/A
pET28-MBP POM121 NLS (291–320) mutant (mut) bearing K313A and K295A mutations in critical residues of major and minor NLS binding sites	Kralt et al., 2015	N/A
pGEX-6P-1 Importin a1	Kralt et al., 2015	N/A
pQE60 Importin ß1	Mitrousis et al., 2008	N/A
pEGFP-N1 POM121 siRNA resistant full length	This paper	N/A
pEGFP-N1 POM121 siRNA resistant POM121 mutant unable to localize to the NPC and bind to Importins lacking amino acids 1–509 (referred as DNPC)	This paper	N/A
Rev-GR-GFP retroviral vector	Rodriguez-Bravo et al., 2014	N/A
GFP tagged NUP62	Genscript	clone ID OHu26446, NM_153719.3 ORF
pGL4.10 reporter	Promega	E6651
pGL4.10 POM121 promoter	This paper	N/A
pGL4.10 POM121 Promoter GBE1 mutant	This paper	N/A
pGL4.10 POM121 Promoter GBE2 mutant	This paper	N/A
pGL4.10 POM121 Promoter GBE3 mutant	This paper	N/A
pRL- Renilla Luciferase Control Reporter Vector	Promega	E2231
pCMV-GATA2	Vidal etal., 2015	N/A
Software and Algorithms		
Prism	GraphPad	https://www.graphpad.com/scientific-software/prism/

REAGENT or RESOURCE	SOURCE	IDENTIFIER
Living Image software v.4.2	PerkinElmer	http://www.perkinelmer.com
SPSS	IBM Analytics	https://www.ibm.com/analytics/spss-statistics-software
GSEA Molecular Signature Database	Broad Institute	https://www.broadinstitute.org/msigdb
DAVID Bioinformatics Resources	David Bioinformatics	https://david.ncifcrf.gov/